Geochemistry Geophysics Geosystems G3

Article
Volume 13, Number 6
23 June 2012
Q06014, doi:10.1029/2012GC004088
ISSN: 1525-2027

Published by AGU and the Geochemical Society

Chalcophile element systematics in volcanic glasses from the northwestern Lau Basin

F. E. Jenner
Department of Terrestrial Magnetism, Carnegie Institution of Washington, Washington, DC 20015-1305, USA (fjenner@dtm.ciw.edu)

R. J. Arculus, J. A. Mavrogenes, N. J. Dyriw, and O. Nebel
Research School of Earth Sciences, Australian National University, Canberra, ACT 0200, Australia

E. H. Hauri
Department of Terrestrial Magnetism, Carnegie Institution of Washington, Washington, DC 20015-1305, USA

[1] The Lau Backarc Basin (S.W. Pacific) hosts numerous spreading centers and rifts, including the Rochambeau Rifts (RR), Northwest Lau Spreading Center (NWLSC), and Central Lau Spreading Center (CLSC). Samples from the NWLSC, RR and CLSC show no evidence for a subduction-derived component in their mantle source regions or evidence for S loss during eruption. The contents of S in glasses from the NWLSC and many from the CLSC and the RR are lower than MORB at a given FeO_{TOT}, indicating melts were initially sulfide-undersaturated. During differentiation, the decrease in Cu and Ag contents at ~7 wt% MgO and the concomitant change in chalcophile element ratios marks the onset of sulfide saturation. The initially sulfide-undersaturated compositions of samples from the NWLSC are attributed to partial melting at pressures higher than parental MORB. The NWLSC and some of the CLSC and RR samples are strikingly enriched in Cu and Ag compared with MORB. This is a characteristic shared by basalts generated in many plume-related tectonic settings. The only plume-related samples that appear to be sulfide-saturated during differentiation and plot within the MORB array are alkaline basalts from the nearby Samoan islands. RR and CLSC basalts have a range in Cu contents, which can be explained by variable mixing between a high-Cu NWLSC-type melt with low-Cu sources from the Samoan plume (RR) and MORB-type mantle (CLSC). The RR alone of these three suites have markedly positive Pb, As, Tl and subtle Mo anomalies, possibly related to assimilation of old, hydrothermally altered, Vitiaz Arc crust.

Components: 16,700 words, 9 figures.

Keywords: Lau Backarc Basin; Samoan plume; basalt; chalcophile; copper; sulfide saturation.

Index Terms: 1036 Geochemistry: Magma chamber processes (3618); 1037 Geochemistry: Magma genesis and partial melting (3619).

Received 3 February 2012; **Revised** 18 April 2012; **Accepted** 14 May 2012; **Published** 23 June 2012.

Jenner, F. E., R. J. Arculus, J. A. Mavrogenes, N. J. Dyriw, O. Nebel, and E. H. Hauri (2012), Chalcophile element systematics in volcanic glasses from the northwestern Lau Basin, *Geochem. Geophys. Geosyst.*, *13*, Q06014, doi:10.1029/2012GC004088.

1. Introduction

[2] The Lau Basin (Figure 1) is a rapidly spreading (~160 mm/yr) backarc basin located west of the Tonga Arc [*Bevis et al.*, 1995; *Taylor et al.*, 1996; *Pelletier et al.*, 1998; *Zellmer and Taylor*, 2001]. Numerous workers have sought to explain the complexity in both major and trace element systematics, plus isotopic variability in samples erupting in this Basin [*Poreda*, 1985; *Loock et al.*, 1990; *Poreda and Craig*, 1992; *Turner and Hawkesworth*, 1998; *Pearce et al.*, 2007; *Keller et al.*, 2008; *Tian et al.*, 2008; *Lupton et al.*, 2009; *Tian et al.*, 2011; *Hahm et al.*, 2012; *Lupton et al.*, 2012a]. In particular, there is a shift in isotopic signatures from 'Pacific'-type mantle in the south, to 'Indian'-type mantle in the northern parts of the Basin, and a conspicuous oceanic island basalt (OIB) signature in isolated parts of the northwestern Lau Basin. Subsequent to the collision of the Ontong Java Plateau with the Vitiaz Trench (~12–10 Ma), subduction of the Pacific Plate ceased along the Solomon-northern Tonga part of the Trench, and the plate margin to the north of Fiji-Tonga became a complex zone of transform faults, rifts and spreading centers (Figure 1). Consequently, mixing of mantle domains that were previously separated by the subducting Pacific Plate is now taking place in the northern part of the Lau Basin [see *Natland*, 1980; *Dunkley*, 1983; *Hamburger and Isacks*, 1987; *Hall*, 2001; *Mantovani et al.*, 2001; *Pearce et al.*, 2007], facilitating southward influx of 'Indian'- (or "SOPITA" [*Staudigel et al.*, 1991; *Pearce et al.*, 2007]) type mantle into the Lau Basin (white arrows, Figure 1b).

[3] Although the mixing of Pacific- and Indian-Type mantle in the northern Lau Basin is generally accepted [*Hergt and Woodhead*, 2007], the nature and extent of the overprinting OIB signature remains enigmatic. Anomalously high $^{3}He/^{4}He$ (up to ~28 R_a), elevated $^{20}Ne/^{22}Ne$ at a given $^{21}Ne/^{22}Ne$ and a range of other geochemical proxies have been used to argue for a Samoan plume contribution to magmas erupting at Rochambeau Bank, the Rochambeau Rifts (RR), the Northwest Lau Spreading Centre (NWLSC), Niuafo'ou Island and the Peggy Ridge [*Lupton and Craig*, 1975; *Volpe et al.*, 1988; *Poreda and Craig*, 1992; *Turner and Hawkesworth*, 1998; *Falloon et al.*, 2007; *Regelous et al.*, 2008; *Lupton et al.*, 2009; *Tian et al.*, 2011; *Hahm et al.*, 2012; *Lupton et al.*, 2012a]. The absence of high $^{3}He/^{4}He$ in magmas erupting at the Central Lau Spreading Center (CLSC) indicates the Samoan plume influence is confined to the northern parts of the Basin. The lateral migration of plume material from the Samoan hot spot (see red arrow on Figure 1b) could follow the western motion of the Pacific Plate at a rate of ~7 cm/yr [e.g., *Koppers et al.*, 2011, and references therein] and become entrained into the Lau Basin by toroidal flow around the edges of the downgoing Pacific Plate [*Schellart*, 2004; *Stegman et al.*, 2006; *Schellart et al.*, 2007]. The absence of high $^{3}He/^{4}He$ in samples from the Mangatolu Triple Junction indicates that the northeastern part of the Lau Basin is isolated from the Samoan plume component by the northern terminus of the Tonga Trench (shown on Figure 1), in accord with tectonic studies of this region [*Zellmer and Taylor*, 2001; *Richards et al.*, 2011]. Hence, the eastern limit of the opening between the northern Lau Basin and Pacific mantle is likely located only slightly east of the RR, where high $^{3}He/^{4}He$ values have been reported.

[4] The high $^{3}He/^{4}He$ and elevated $^{20}Ne/^{22}Ne$ at a given $^{21}Ne/^{22}Ne$ of magmas presently erupting at the NWLSC, the RR and surrounding area can be used to argue for a primitive undegassed mantle component beneath the northern Lau Basin. However, understanding the origin of this component using isotopic systematics (e.g., Sr-Nd-Pb) is complicated, because the composition of primitive mantle lies within the convergence, or focus zone (FOZO [*Hart et al.*, 1992]) of the four mantle end-member compositions (i.e., depleted mantle, HIMU, EM1 and EM2 [see *Workman et al.*, 2004, Figure 5]. Hence, alternative tracers are required to understand the origin and distribution of the sources of the RR and NWLSC magmas, which are independent from those of the CLSC magmas. Mixing of a Samoan component with the surrounding Indian-Type mantle (see *Tian et al.* [2011] for an example of possible mixing models) should affect numerous trace element characteristics, but this is not observed or is unconvincing. For example, samples from the Mangatolu Triple Junction, Peggy Ridge, Rochambeau Bank and Niuafo'ou Island have Gd/Yb comparable to MORB [see *Tian et al.*, 2011, Figure 4] as opposed to the extremely high Gd/Yb typical of Samoan magmas with residual garnet in the mantle source [see *Jackson et al.*, 2010, Figure 4].

[5] In addition to mixing of source components, the compositions of the magmas erupting at the RR and vicinity could be complicated by crustal contamination. The areas shallower (water depth) than 2000 m in the northern part of the Lau Basin

trend approximately parallel to the paleo-Vitiaz Trench (Figure 1a) at comparable distances to those observed between the Tonga Ridge and the Tonga Trench. Conceivably, the ocean floor in the northern part of the Lau Basin is the stretched and boudinaged basement of the Paleogene-early Neogene Vitiaz Arc. The absence of clear correlation between $^{3}He/^{4}He$ and other isotopic systems in magmas erupting at and around the RR may indicate the parental magmas are contaminated by variable mixing with a basement of crustal material produced during the active stage of the Vitiaz Arc. The trend to high-$^{87}Sr/^{86}Sr$ and low-$^{143}Nd/^{144}Nd$ of some magmas erupting at Rochambeau Bank and Niuafo'ou Island is consistent with ingress of a Samoan plume component [i.e., *Tian et al.*, 2011]. Alternatively, this component may have been inherited by introduction of Samoan-derived, high-$^{87}Sr/^{86}Sr$ volcaniclastic sediments to the mantle wedge during previous stages of subduction along the Vitiaz Trench, and/or crustal contamination during ascent of the parental magmas from high $^{87}Sr/^{86}Sr$ arc magmas comprising the Vitiaz Arc crust. Indeed, the diffusively extended topography of the RR indicates the evolution of this area is not just a simple spreading ridge, unlike the linear structure observed at the NWLSC (Figure 2), which is more distal from the Paleo-Vitiaz Trench (Figure 1). Hence, samples from the NWLSC, which also have elevated $^{3}He/^{4}He$ ranging from 7.4 to 20.8 R_a, provide an ideal opportunity for constraining the nature of the OIB component, which can be compared with the potentially more complicated RR samples.

[6] Here we present major and trace element compositions for samples from the RR, NWLSC, and CLSC (Table S1 in the auxiliary material).[1] Samples were recovered during the SS07/2008 research voyage (NoLauVE) of the Australian Marine National Facility RV *Southern Surveyor*.

[1]Auxiliary materials are available in the HTML. doi:10.1029/2012GC004088.

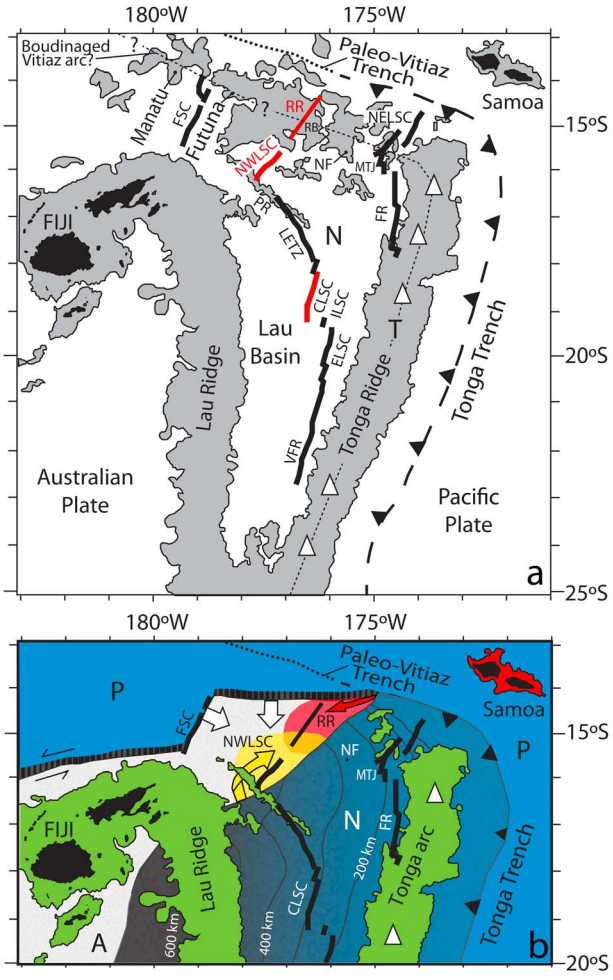

Figure 1. (a) Map showing the major tectonic features of the Lau Basin. Areas shallower than 2000 m are shaded gray (adapted from map provided in *Martinez and Taylor* [2003]). Data presented in this study are from (shown in red) the North West Lau Spreading Centre (NWLSC), the Rochambeau Rifts (RR) and the Central Lau Spreading Centre (CLSC). Also shown are the locations of: Rochambeau Bank (RB), Valu Fa Ridge (VFR), Niuafo'ou Island (NF), Mangatolu Triple Junction (MTJ), Northeastern Lau Spreading Centre (NELSC), Fonualei Rifts (FR), East Lau Spreading Centre (ELSC), Futuna Spreading Centre (FSC), Intermediate Lau Spreading Centre (ILSC), Peggy Ridge (PR), Lau Extensional Transform Zone (LETZ), Tonga Plate (T) and Niuafo'ou Plate (N). The approximate location of the Paleo-Vitiaz Trench is shown as a dotted line extending west from the presently active Tonga Trench. Triangles along the dotted line show the approximate location of the subaerial volcanoes of the presently active Tonga arc. Notably, the areas shallower than 2000 m in the northern part of the Lau Basin trend approximately parallel to the Paleo Vitiaz Trench, indicating that this area may be the boudinaged basement of the Paleogene to early Neogene Vitiaz arc. (b). Schematic map outlining the boundaries of the major and minor plates in the region, including the subducted portion of the Pacific Plate projected to the surface based on the contouring of the seismicity [*Benz et al.*, 2011]. Abbreviations are: A: Australian Plate; N: Niuafo'ou Plate; P: Pacific Plate. Arrows show the inferred mantle flow directions; red arrow, toroidal flow of the Samoan plume component; white arrow, flow of Indian-type mantle into the northern Lau Basin; and yellow arrow, poloidal flow or material around the edge of the Pacific Plate.

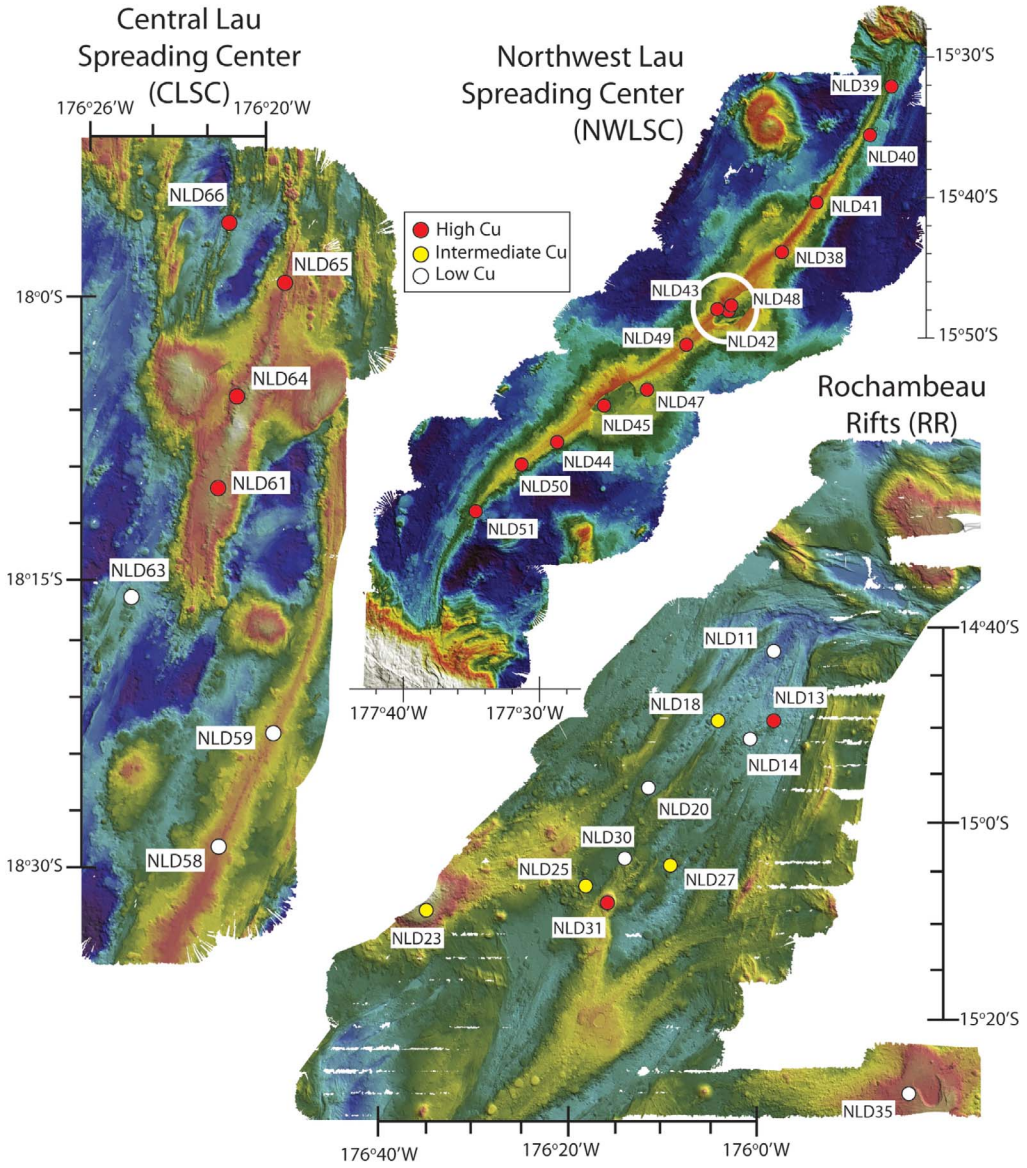

Figure 2. Multibeam sonar swath maps of the RR, NWLSC, and CLSC showing sample locations. Depths range from ~2400 m (deep blue) to 1900 m (red). Bathymetric mapping of the Northwest Lau Backarc Basin was undertaken with a Kongsberg Simrad EM300 multibeam system, comprising a 1° by 1° set of 135 beams clustered around a 30 kHz frequency. Real-time beam steering compensation was made for ship motion. Motion sensing and positional navigation had accuracies of (less than or equal) 0.02° and ±5 m respectively. Bathymetry and backscatter data were edited and gridded on-board at a variety of cell sizes with Caris software. For the images shown in Figure 2, a 25 m cell-size was used having a vertical resolution of 1–2 m in the water depths of ~2000 m that characterize most of the terrain in this portion of the Basin. Open white circle on the map of the NWLSC shows the location of samples erupting with the most depleted LREE patterns, indicating more pronounced rates of melt extraction at the central part of the NWLSC.

Major (EMPA) and trace element analyses (LA-ICP-MS) for these samples were undertaken at the Research School of Earth Sciences, Australian National University, following methods described in previous contributions [*Jenner et al.*, 2009; *Jenner and O'Neill*, 2012b, 2012a]. The data presented here for samples from the RR, NWLSC, and CLSC contain the typical set of trace elements used to understand the petrogenesis of basaltic magmas (i.e., rare earth elements (REE), large ion lithophile elements (LILE), high field strength elements (HFSE), the first row transition elements (FRTE), and a selection of less commonly analyzed elements (i.e., Li, Be, Ge, Ga, As, Se, Mo, Ag, Cd, In, Sn, Sb,

W, Re, Tl, and Bi), which are used here to provide additional constraints on mantle source characteristics. The tectonic setting in which the samples from the RR, NWLSC, and CLSC are generated is complex: backarc basin samples with potential plume, MORB-source, subduction-related and crustal inputs. Hence, data for samples from these centers and rifts are compared against a complementary data set of analyses of ocean floor basalts from a range of fracture zones and spreading ridges from the Pacific, Atlantic, and Indian Oceans (data from *Jenner and O'Neill* [2012a]), collectively referred to here as mid-ocean ridge basalts (MORB), for ease of reference. Data sets of analyses that include the total range in trace elements reported herein are currently unavailable for samples from the Samoa subaerial and submarine chain. Hence, we present new analyses of ten sub-aerially erupted volcanic glasses from a single lava flow of the Pu'u'O'o eruption (11.30 A.M., 1 November 2000), Kilauea volcano, Hawaii [see *Garcia et al.*, 2000; *Pietruszka et al.*, 2006] as an example of typical OIB (Table S1). We include for comparison, selected elemental data (Nb, Yb and Th; Table S2) for samples from ridges and rifts in the eastern Lau Basin (Valu Fa and Fonualei) with a well-defined subduction input.

[7] Since the publication of the Pual Ridge and vicinity, Eastern Manus Backarc Basin data set (*Jenner et al.* [2010] referred to in the following text as the Manus Basin), there have been improvements in calibration values (NIST SRM 612) and analytical protocols for LA-ICP-MS techniques [see *Jenner and O'Neill*, 2012b]. Hence, the data presented in *Jenner et al.* [2010] are updated and presented here (Table S3) as an example of an arc-proximal backarc sample suite with a strong subduction influence, and as a complementary extension to the global ocean floor basaltic data file of *Jenner and O'Neill* [2012a]. Pervasive degassing during eruption of samples from the Manus Basin resulted in loss of S to levels close to the limit of detection of the electron microprobe [*Jenner et al.*, 2010]. Hence, we present more precise data for low S contents in samples from the Manus Basin (Table S3), together with Cl, CO_2, H_2O and F, using the Cameca IMS 6f ion microprobe housed at the Department of Terrestrial Magnetism, following the techniques described in *Hauri et al.* [2002].

2. Results

[8] Samples from the NWLSC are basaltic in composition, except NLD39 and NLD41, which are classified as basaltic andesite and andesite, respectively. FeO_{TOT}, TiO_2, V, Re, S and Se in the NWLSC show a systematic increase in contents with decreasing MgO, until ~5 wt.% MgO, followed by a marked drop in contents with further decreases in MgO (Figure 3). Glasses from the NWLSC are characterized by very high Cu contents, and consistently higher Ag, and Re at a given MgO compared with MORB (Figure 3) and primitive mantle values (PM values from *Palme and O'Neill* [2003]) of Re (0.32 ppb), Cu (20 ppm) and Ag (4 ppb). Cu and Ag contents show a subtle increase with decreasing MgO from 8.7 to ~7 wt.% MgO, followed by a progressive decrease in samples with <7 wt.% MgO (Figure 3). Basaltic glasses from the RR and CLSC have a more limited range in MgO contents compared to samples from the NWLSC (Figure 3). Additionally, the most MgO-rich samples from the RR have slightly higher TiO_2 and S, lower V and Cu, and display less coherent trends in compositions compared to samples from the NWLSC (Figure 3). Samples from the CLSC can be distinguished from those collected from the NWLSC and the RR by the consistently lower TiO_2 contents at a given MgO (Figure 3b), have a similar range in Cu contents to samples from the RR (Figure 3g) and lack a coherent fractionation trend. Our limited sample set from Hawaii has a restricted compositional range that can be distinguished from samples from the NWLSC, RR and CLSC by the higher TiO_2 at a given MgO, but with FeO_{TOT} and V contents comparable to those from the RR (Figure 3). In addition to samples from the NWLSC and a number of samples from both the RR and CLSC, samples from Hawaii have elevated Cu and Ag contents compared to the MORB array.

[9] Trace element abundances normalized to PM of samples from the NWLSC, RR, CLSC and Hawaii are shown in Figure 4. In addition to the typical range in elements presented on PM-normalized diagrams, we have extended the list to include analyses of Be, Zn, Ge, Ga, As, Mo, Cd, In, Sn, Sb, W, Tl and Bi to establish whether these elements can be used to place further constraints on the petrogenesis of the suites of samples from the NWLSC, RR, and CLSC. To avoid additional congestion, the trace elements displayed in Figure 3 are not included in Figure 4. The additional elements have been added to the traditional sequence (intended to span from highly to mildly incompatible relative to a peridotite assemblage) in their 'approximate' positions with respect to their incompatibility relative to refractory lithophile elements (i.e., As, Mo,

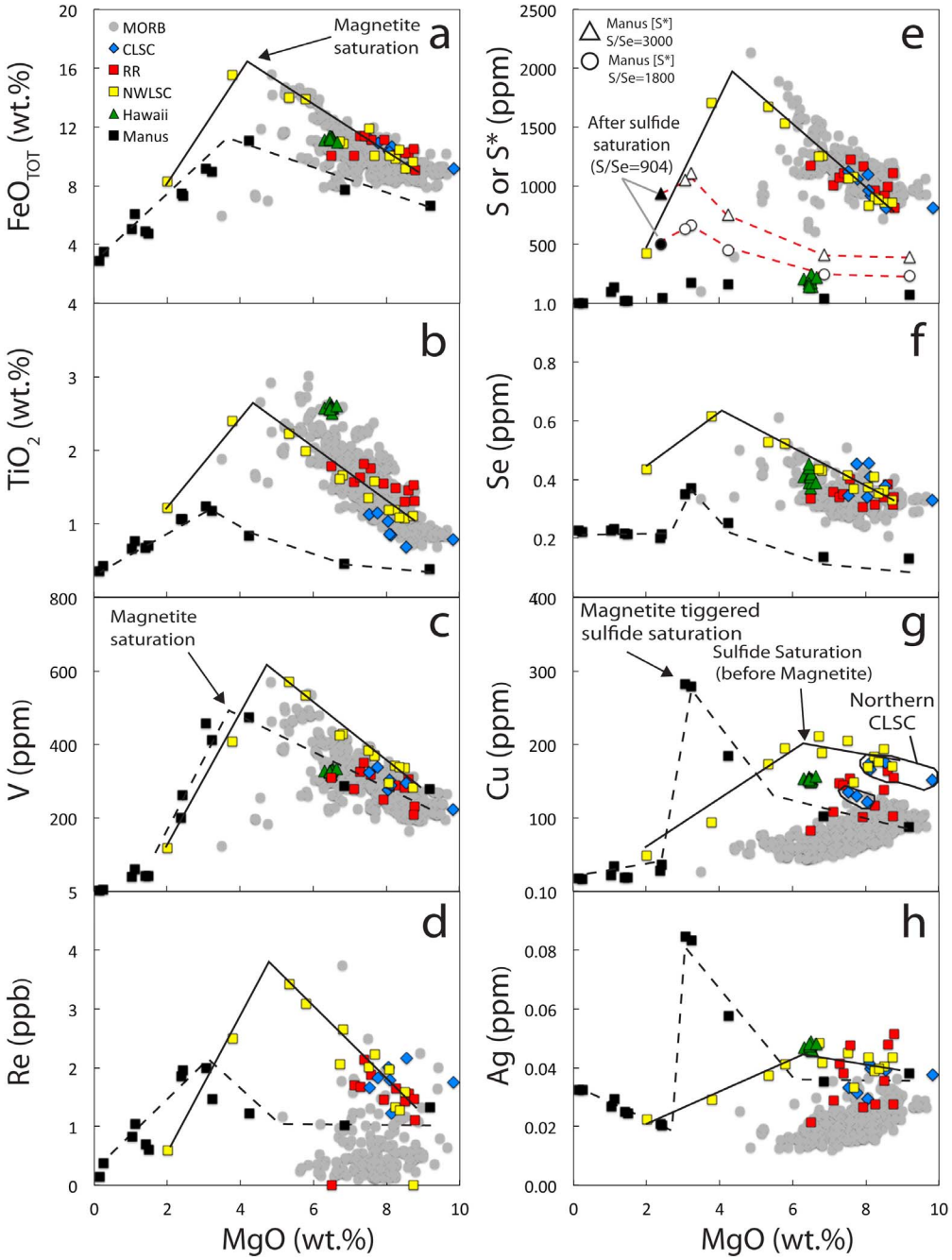

Figure 3. Major and trace element variations versus MgO for samples from the NWLSC, RR, CLSC, Hawaii and Manus Basin compared to MORB. Data for MORB from *Jenner and O'Neill* [2012a]. Data from the Manus Basin updated from *Jenner et al.* [2010] following improvements to analytical accuracy [see *Jenner and O'Neill*, 2012b]. Inferred liquid lines of decent for the samples from the NWLSC and the Manus Basin (black lines) are given to highlight the trends discussed in the text. The estimated (prior to degassing) content of S in the Manus samples [S*] prior to sulfide saturation (open circles and triangles) = [Se] × $(S/Se)^{primitive\ melt}$, calculated using two estimates of the initial S/Se in the primitive melt; 3000 (MORB-like) and 1800 (mantle source more depleted than MORB). Red dashed lines show the modeled changes in S* during evolution of the melt. S* after sulfide saturation (black circles and triangles) = $S^{*before\ sulfide\ saturation}$ − ΔS* (ΔS* = decrease in S content following sulfide saturation), where ΔS* = [ΔSe] × $S/Se^{bornite}$ (calculated using the drop in [Se] between samples MD7 and MD8).

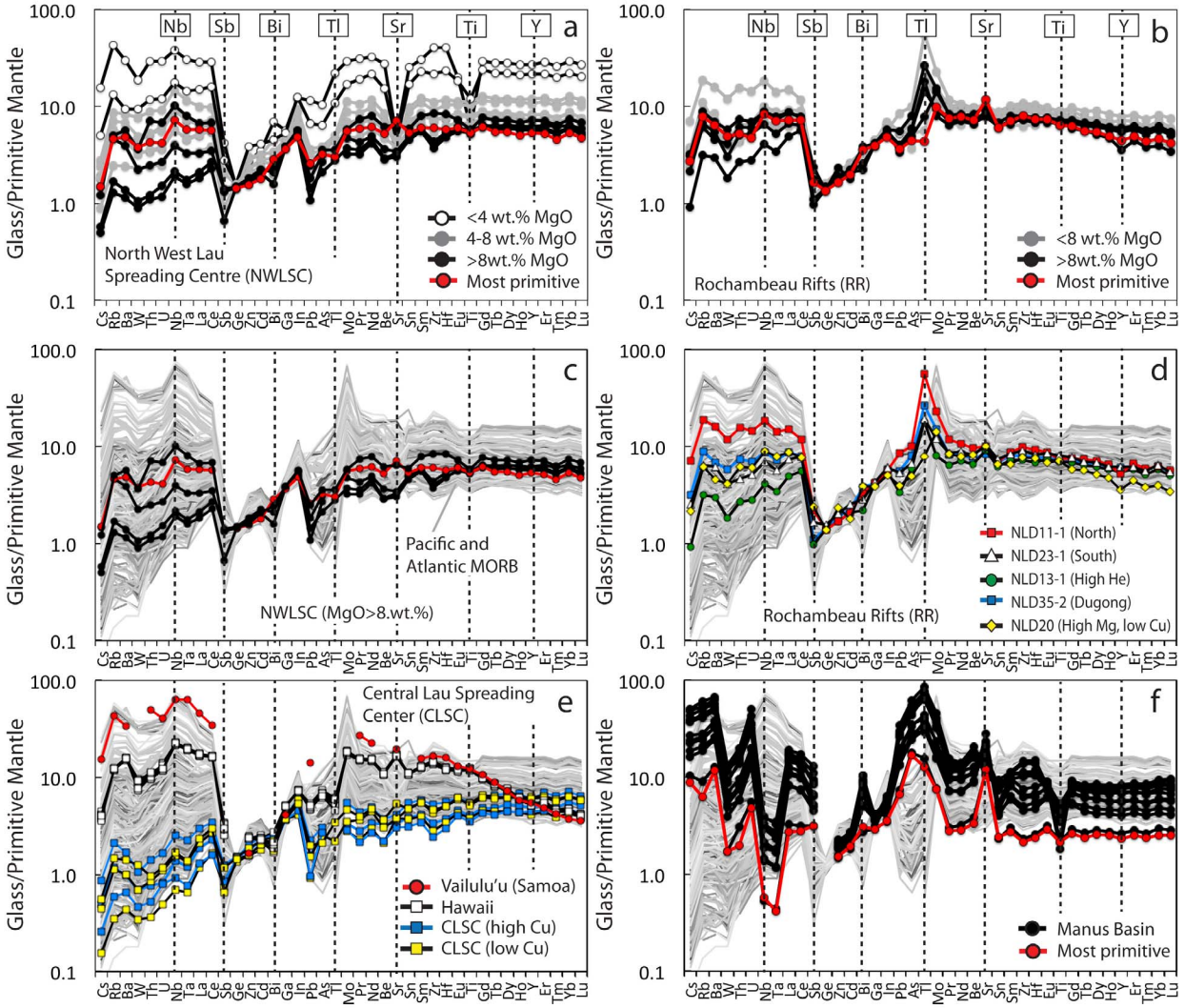

Figure 4. Primitive mantle-normalized plots showing trace element compositions of samples from: (a) the NWLSC; (b) the RR, (c) samples from the NWLSC with >8 wt.% MgO compared to the MORB array (MORB data from *Jenner and O'Neill* [2012a]); (d) comparison of the compositions of a range of samples from the RR compared to MORB; (e) Hawaii and Samoa (average data for Samoan volcanoes from *Workman et al.* [2004]) compared to MORB; (f) the Manus Basin.

Sn, Sb and Pb between refractory lithophile elements Ce and Pr [e.g., *Palme and O'Neill*, 2003]. However, the overall ordering of the chalcophile/siderophile elements that are displayed on Figure 4 (i.e., Mo, As, Sb, Ge, Sn, In, Bi, Pb and Tl positioned between Ce and Pr) is chosen as a means for demonstrating the range in compositions of samples presented here by achieving a coherent trend between Sb and Mo on Figure 4 for samples from the NWLSC, RR and CLSC compared with MORB, as opposed to providing a definitive ordering with regards to compatibility.

[10] NWLSC glasses have flat HREE patterns (Gd/Yb_{PM} ranging from 0.99 to 1.15), are variably depleted in LREE (La/Sm_{PM} ranging from 0.33 to 0.95), have positive Nb anomalies relative to Ta and U, variable enrichments in Rb and Ba relative to Cs and W, and depletions in Pb and As relative to In and Pr (Figure 4a). With decreasing MgO content, samples show progressively increasing negative Sr, Eu and Ti anomalies compared to neighboring REE on primitive mantle-normalized plots, and an overall increase in abundances of trace elements. RR glasses display a narrower range in trace element contents and higher Gd/Yb_{PM} (1.15–1.48) compared to samples from the NWLSC (Figure 4b), are LREE-depleted to enriched (La/Sm_{PM} = 0.68–1.73), have Nb enrichments relative to U and Ta comparable to samples from the NWLSC and

MORB, and show variable enrichments in Rb, Ba, and Sr, and depletions in Y compared to samples from the NWLSC. A striking feature of the RR samples are the positive Tl spikes and the less pronounced, or absent, Pb and As depletions relative to In and Pr when compared to both MORB and samples from the NWLSC (Figures 4c and 4d).

[11] The CLSC samples are broadly similar to the most depleted MORB in terms of the range from incompatible to relatively compatible trace element abundances (Figure 4e), with a range in La/Sm_{PM} from 0.30 to 0.51, and depleted to enriched HREE patterns (Gd/Yb_{PM} range form 0.87–1.06). Samples from the CLSC show depletions in Pb and As relative to In and Pr, and enrichments in Nb relative to U and Ta, similar to MORB and samples from the NWLSC. The NWLSC and CLSC samples have considerably smoother trace element patterns from Sb to In, and RR from Sb to As, compared to the MORB array (MORB show pronounced depletions in Sb, Ge and Bi relative to Zn and Cd, and typically more pronounced depletions in As relative to Tl). In addition, samples from the NWLSC, Hawaii, and many of the samples from the CLSC lack the distinctive positive Mo anomalies relative to Tl and Pr of MORB. In contrast, the RR have enrichments in Mo relative to Pr. Hawaiian basalts have trace element patterns from Cs to In similar to samples from the NWLSC (Figure 4e) and the more LREE-enriched MORB samples. However, the HREE patterns are highly fractionated (Gd/Yb_{PM} = 2.12–2.21) compared to the NWLSC, RR, and CLSC (Figure 4e). Hawaiian glasses show depletions in Tl relative to As and Mo, and subtle enrichments of Sr relative to Be and Sn.

3. Source Characteristics of MORB, Hawaii and the Manus Basin Magmas

[12] The spectrum of MORB compositions (Figure 4) with a continuum from LREE-enriched to depleted character provides an important comparator for the Lau Basin samples. We note this continuum renders any presentation of a normal-MORB (NMORB), enriched MORB (EMORB), or average MORB value for normalization purposes as likely misleading [*Hofmann*, 2003; *Jenner and O'Neill*, 2012a]. Hence, we use the entire MORB array plotted against PM to embrace the entire range in compositions generated at mid-ocean ridges (Figure 4) for comparison with samples generated in other tectonic settings, as opposed to the use of NMORB-normalized plots.

[13] In the context of this contribution, we note MORB are characterized by enrichments in Rb and Ba relative to Cs and W, enrichments in Nb relative to Ta and U, and depletions in chalcophile elements Sb, Ge, Bi, Pb, As and Tl relative to Ce when compared to PM. MORB show a striking enrichment in Mo relative to both Ce ($Mo/Ce_{PM} = 2.26 \pm 0.49$) and Pr ($Mo/Pr_{PM} = 2.15 \pm 0.49$), despite their similar incompatibilities during differentiation of basaltic melts [*Newsom et al.*, 1986; *Sims et al.*, 1990; *Fitton*, 1995; *Jenner and O'Neill*, 2012a], indicating the higher incompatibility of Mo compared to both Ce and Pr during melting of the MORB source mantle. Alternatively, the high Mo/Ce and Mo/Pr of MORB compared to PM may indicate the PM value for Mo is too high, and the method for estimating the Mo content of PM needs to be reassessed. Samples from Hawaii have trace element patterns comparable with the most LREE-enriched MORB (Figure 4e), with the exception of the highly fractionated HREE patterns of the former, demonstrating the presence of residual garnet in their mantle source region during melt extraction at high pressures [e.g., *Chen et al.*, 1991]. A notable difference between the trace element patterns of MORB compared to samples from Hawaii are the absence of Mo anomalies relative to Ce (Mo/Ce_{PM} = 1.06–1.15) and Pr (Mo/Pr_{PM} = 1.13–1.25), possibly indicating the compatibility of Mo in garnet, although to the authors' knowledge, appropriate partition coefficients for Mo between garnet and silicate melt are currently unavailable to test this hypothesis.

[14] In contrast to MORB and Hawaii, arc-proximal Manus Basin samples (Figure 4f) show enrichments in Cs, U and Pb compared to LREE, Sr relative to Nd, and pronounced depletions in Nb and Ta relative to La, typical of convergent margin basalts [e.g., *Plank and Langmuir*, 1988; *Chauvel et al.*, 1995; *Morris and Ryan*, 2003; *Pearce et al.*, 2005; *Plank*, 2005]. In addition, subduction-related basalts from the Manus Basin have enrichments in Bi relative to Ga, As, and Tl relative to Pr, and substantially higher Sb/Ce compared to PM, MORB, and Hawaii. The enrichment of As, Tl and Sb in subduction- related magmas compared to MORB is consistent with previous studies [*Noll et al.*, 1996; *Hattori et al.*, 2002]. In contrast, Mo is not enriched in the Manus Basin suite: the Mo/Ce_{PM} ranges from 1.60 to 2.69, and Mo/Pr_{PM} from 1.62 to 2.94, similar to the range of MORB values, indicating only limited mobility of Mo during subduction-related processes. The enrichment of some chalcophile/siderophile trace elements in samples from the

Manus Basin (As, Sb, Tl, Bi and Pb), but depletions or MORB-like abundances in others (S, Se, Cu, Ag and Mo; Figures 3 and 4), indicates the processes controlling the behavior of these elements in the subducted slab and mantle wedge are distinct from the mantle source region of MORB. Geochemical studies of pristine and hydrothermally altered oceanic crust, and black smoker-type hydrothermal fluids have shown Tl is particularly susceptible to leaching during hydrothermal alteration by high temperature (>250–300°C) fluids [*Nielsen et al.*, 2006]. Similarly, trace element analyses of sulfides associated with black smokers and other types of hydrothermal deposits have noted enrichments in As, Sb, Tl, Bi and Pb [*Hannington et al.*, 1991; *Shin et al.*, 2004; *Kristall et al.*, 2011]. Hence, enrichment of the mantle wedge via subduction of hydrothermally altered oceanic crust and associated low-temperature As-Sb-Tl-Bi-Pb sulfides, as previously suggested to explain the enrichments in Pb in arc magmas and the continental crust compared to MORB [*Chauvel et al.*, 1995], could explain the enrichment of the source region of the Manus Basin magmas in these chalcophile elements relative to others such as Cu, Ag. Alternatively, the processes taking place during black-smoker type hydrothermal alteration may be resulting in the leaching of As, Sb, Tl, Bi and Pb relative to the REE from the oceanic crust during subduction, but on a considerably larger scale than observed on the seafloor.

[15] During differentiation of MORB magmas, the contents of both Cu and Ag decrease with decreasing MgO, consistent with the removal of sulfide liquid during differentiation (Figure 3). The lack of enrichment of Cu and Ag in the primitive Manus Basin samples compared to MORB, as previously demonstrated by *Jenner et al.* [2010], may indicate these magmatic sulfides reside in the gabbroic layers of the oceanic crust (~1–2 km depth beneath the ocean floor [see *Klein*, 2003]) and as a consequence, have little impact on the budget of chalcophile elements supplied to the mantle wedge during subduction (i.e., they are located too deep in the oceanic crust).

4. Source Characteristics of the Northwestern Lau Basin Magmas

[16] On PM-normalized plots, samples from the NWLSC, CLSC, and RR show a number of notable geochemical characteristics compared with the MORB spectrum. For example, samples from the NWLSC lack positive Zn, Cd and Mo anomalies; the CLSC basalts show only subtle enrichments in Mo; and RR basalts have distinctively smooth trace element patterns between Sb and As compared to MORB (Figure 4). Similarly, the elevated Re, Cu, and Ag contents at a given MgO indicate the petrogenesis of the samples from the NWLSC and a number of samples from the RR and CLSC was distinct from that of MORB (Figure 3). In contrast to Hawaiian basalts, the most primitive samples from the NWLSC (>8 wt.%) have relatively flat HREE patterns, which are comparable to typical MORB (Gd/Yb_{PM} = 1.00–1.15), indicating that garnet was not a residual phase in the mantle source region during partial melting. However, the most primitive samples from the CLSC (Gd/Yb_{PM} = 0.87–1.06) and the RR (Gd/Yb_{PM} = 1.15–1.48), have a range in HREE abundances, indicating the involvement of residual garnet in their mantle source regions at some stage during their petrogenesis, either in the source mantle (i.e., prior melting of the mantle source region of the CLSC magmas within the garnet stability field to achieve the low Gd/Yb_{PM} during subsequent melting) or during melt extraction (i.e., to achieve the high Gd/Yb_{PM} of a number of samples from the RR). Nevertheless, the elevated Gd/Yb_{PM} of samples from the RR are less pronounced than samples from Hawaii and Samoa (Figure 4e). Hence, samples from the NWLSC, CLSC, and RR are geochemically distinct from MORB and Hawaiian basalts. However, we note the samples from Hawaii are also enriched in Cu and Ag at a given MgO compared to the MORB array, which is a distinctive feature of samples presented here from the NWLSC (Figure 3).

[17] Neither the CLSC, NWLSC, nor the RR samples have the strong enrichments in Cs and U or depletions in Nb and Ta relative to neighboring elements on PM-normalized plots, characteristic of subduction-related volcanic rocks, such as those from the Manus Basin (Figure 4f). Additionally, PM-normalized patterns for samples from the NWLSC and CLSC (Figures 4a and 4e) show depletions in Pb, As, and Tl relative to In and Pr, which are completely different to the geochemical signatures of subduction-related magmas from the Manus Basin. The lack of a subduction-derived input to the source region of the CLSC, NWLSC, and RR magmas can also be demonstrated on a plot of Th/Yb versus Nb/Yb (Figure 5). The majority of these samples plot within the MORB array, from relatively depleted (CLSC) through moderate (NWLSC) to enriched character (RR), whereas volcanic glasses from the Pual Ridge region of the Manus Basin, the Fonualei and Valu Fa Rifts

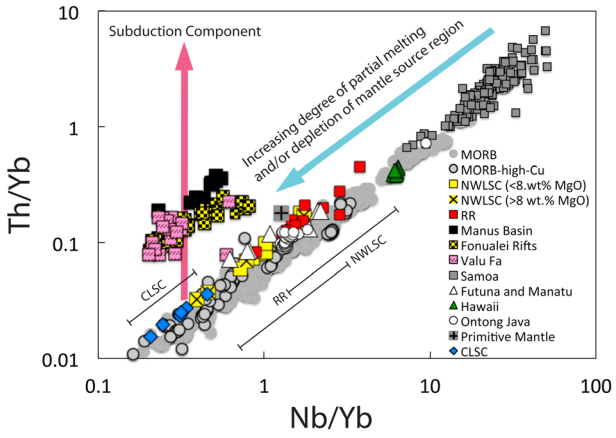

Figure 5. Th/Yb versus Nb/Yb. Data sources: MORB [*Jenner and O'Neill*, 2012a], Samoa [*Hart et al.*, 2004; *Workman et al.*, 2004; *Jackson et al.*, 2010], Fonualei and Valu Fa Rifts, unpublished. Ontong Java [*Fitton and Godard*, 2004], Futuna and Manatu [*Jackson et al.*, 2010]. Samples from *Jenner and O'Neill* [2012a] that were distinguished as having high Cu contents at a given MgO (their Figure 3d) are shown. PM values from *Palme and O'Neill* [2003].

(eastern Lau Basin) have elevated Th/Yb at a given Nb/Yb compared to the MORB array, resulting from the mobility of Th relative to Nb during subduction-related processes [e.g., *Pearce*, 2008]. Trace element compositions of samples from the CLSC, NWLSC, and RR show no evidence in terms of established trace element criteria for crustal contamination and/or enrichment of the mantle source region by a subduction-derived component. The lack of evidence for a subduction component to the mantle source region of the NWLSC and the RR magmas is in agreement with plate reconstructions based on earthquake distributions [*Benz et al.*, 2011; *Richards et al.*, 2011], which indicate the northern limit of the subducting Pacific Plate is located south of both the NWLSC and the RR (Figure 1b). Samples from the RR are geochemically distinct from those retrieved from the NWLSC and the CLSC because of the elevated Pb and As relative to In and Pr, and pronounced spikes in Tl and Mo relative to Pr on PM-normalized plots (Figures 4b and 4d). These specific characteristics are comparable to those displayed by the subduction-related samples from the Manus Basin. However, the lack of other diagnostic trace element patterns of subduction-related basaltic magmatism suggests an alternative origin for these specific chalcophile element enrichments, which will be discussed below. In contrast to the RR and NWLSC, the CLSC is located directly above the subducting Pacific Plate (Figure 1b) and despite the highly depleted compositions of the erupting magmas (i.e., the extremely low incompatible element contents, making them particularly susceptible to overprinting by subduction-derived fluids or melts; Figure 4), these samples also show no trace element evidence of a subduction-zone signature. Hence, we infer the Pacific Plate surface temperature increased from ~730°C below the Tonga arc (slab depth = 123 km) to ≥900°C by a depth of ~300 km, resulting in the destruction of the key volatile-hosting phases such as phengite, allanite and monazite [*Hermann and Spandler*, 2008; *Klimm et al.*, 2008; *Skora and Blundy*, 2010; *Syracuse et al.*, 2010; *Cooper et al.*, 2012; *Ruscitto et al.*, 2012]. We conclude there is no unequivocal evidence for involvement of subducted Pacific Plate components in the mantle source regions as west as the RR, NWLSC or the CLSC.

5. Mantle Source Variability

[18] Samples from the CLSC, NWLSC, and RR have a large range in incompatible element contents and ratios (Figures 4 and 5). Even within the NWLSC sample set containing >8 wt.% MgO, there is a high degree of variability in trace element patterns (Figure 4c). In terms of Nb/Yb versus Th/Yb, the most primitive magmas from the NWLSC (>8 wt.% MgO) have a range in compositions spanning almost half the entire MORB array (Figure 5). The lack of a subduction-related input to the source region of the CLSC, NWLSC, and RR magmas indicates the variability can be attributed either to progressive depletion of the mantle source region, variations in the degree of partial melting, and/or variable mixing with an enriched OIB end-member composition (the Samoan plume).

[19] The high MgO contents of the most mafic samples (>8 wt.%), which occur along the length of the NWLSC (Figure 6a), indicates the parental magmas were generated by similar degrees of partial melting. The range in LREE patterns (e.g., La/Sm from 0.33 to 0.95) within the five most mafic samples is too large to be attributed to single magma chamber processes, such as fractional crystallization, because of the limited range in MgO contents. Figure 6b shows the melts erupting along the NWLSC, in particular the samples with >8 wt.% MgO, have systematically lower La/Sm in the central, relatively shallow parts of the Center (Figure 2, samples enclosed within the white circle), compared

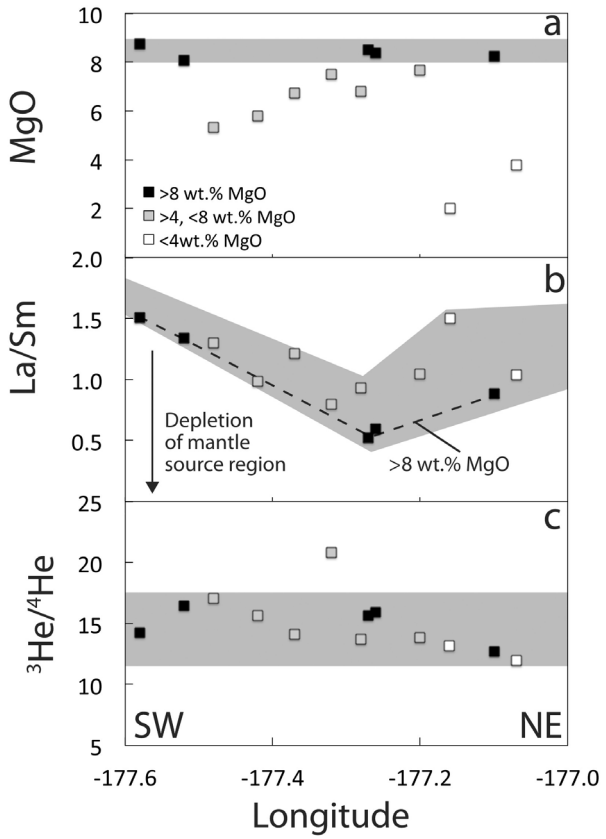

Figure 6. Variations in (a) MgO, (b) La/Sm and (c) $^{3}He/^{4}He$ ($^{3}He/^{4}He$ data from *Lupton et al.* [2009]) versus longitude for samples from the NWLSC. Basalts with >8 wt.% MgO erupt along the length of the NWLSC, indicating the range in major element compositions is a result of fractional crystallization as opposed to varying degrees of partial melting. La/Sm show a trend to lower values in the central part of the NWLSC (corresponding to the white open circle on Figure 2), indicating the degree of melt production and consequently, depletion of the mantle source region was highest in the center of the NWLSC, causing lower La/Sm. There is no correlation between $^{3}He/^{4}He$ versus longitude, demonstrating $^{3}He/^{4}He$ is unaffected by the degree of short–term depletion of the mantle source region.

to the deeper northeastern and southwestern tips. The distribution in La/Sm (shaded fields on Figure 6b) indicates melt production/extraction was greater toward the middle of the NWLSC, resulting in a more rapid short-term depletion of the mantle source region feeding magmatism in this area compared with the propagating tips. Alternatively, the high La/Sm, Nb/Yb and Th/Yb could be attributed to mixing with a Samoan OIB component, as suggested for samples from the RR and surrounding area [*Tian et al.*, 2011]. If lateral migration of the Samoan component is responsible for the range in La/Sm, Nb/Yb, and Th/Yb of NWLSC samples, these ratios would be expected to decrease from NE to SW along the rift. This is not observed so we attribute the range in La/Sm, Nb/Yb and Th/Yb of NWLSC samples to variable degrees of melt extraction and depletion of the underlying mantle source region.

[20] In contrast to La/Sm, $^{3}He/^{4}He$ remains approximately constant along the length of the Center, at values notably higher than typical MORB [see *Lupton et al.*, 2009], consistent with variable degrees of partial melting of a specific source mantle. Trace element abundances of samples from the Lau Basin show only weak correlations with variations in radiogenic isotopic systems, such as Nd, Sr, and Hf [e.g., *Pearce et al.*, 2007; *Tian et al.*, 2011]. We suggest rapid opening of the Lau Basin, resulting in pervasive melt extraction and localized variations in trace element proxies of mantle depletion, as exemplified by samples from the NWLSC, is likely the major variable contributing to the weak correlations between trace element and isotopic systematics.

[21] Samples from the southern parts of the overlapping rifts forming the CLSC (white symbols, Figure 2) have slightly higher Gd/Yb_{PM} and lower La/Sm_{PM} (Gd/Yb_{PM} ranging from 0.98 to 1.06 and La/Sm_{PM} of 0.30–0.43, respectively) compared to samples from the northern parts of the CLSC (Gd/Yb_{PM} of 0.87–0.92 and La/Sm_{PM} of 0.38–0.51, respectively; red symbols on Figure 2). Additionally, northern samples from the CLSC have consistently higher Cu and Ag contents at a given MgO compared to southern samples (distinguished on Figures 3g and 4e). The subtle geochemical differences for samples from the CLSC, which can be related to their geographic locations, indicate slight variations in the petrogenesis of magmas erupting along the CLSC, which may be linked to the ages of the rifts. Samples from the RR show no clear correlations between La/Sm and Gd/Yb with either latitude or longitude. The samples with Cu contents at a given MgO that plot above the MORB array are typically erupting in the southern parts of the RR (closest to the NWLSC; yellow and red symbols on Figure 2), however the correlation is less pronounced compared to the systematic geochemical variations of CLSC and NWLSC magmas. Hence, samples from the NLWSC, CLSC and RR preserve evidence for complex trace element systematics, which can be linked to either compositional differences between the mantle source regions (e.g., the CLSC and the RR) or the evolution of the mantle source region during progressive melt extraction

(e.g., the NWLSC). Additionally, RR samples have consistently lower V and higher Ti contents at a given MgO (notably comparable to Hawaiian basalts, Figure 3), indicating the parental magmas of the NWLSC and the RR were compositionally distinct, possibly as a result of redox variability [*Mallmann and O'Neill*, 2009] and/or source mixing. The lower TiO_2 of the CLSC samples (Figure 3b), coupled with the extremely low Nb/Yb and Th/Yb (Figure 5) demonstrates the mantle source region of the CLSC magmas was more depleted than the source of both the NWLSC and RR magmas.

[22] Using the highest MgO samples from each spreading center, their respective Nb contents and the lack of discernable differences in primary CO_2/Nb between mantle sources characterized by high $^3He/^4He$ and MORB-like ratios in samples from the Lau Basin [*Hahm et al.*, 2012], we can calculate CO_2 fluxes assuming a mantle source CO_2/Nb of 530 similar to average undegassed MORB [*Cartigny et al.*, 2008]. With magma production rates estimated for each area of 0.033 km^3/yr (RR and NWLSC) to 0.12 km^3/yr for CLSC [*Taylor et al.*, 1996; *Crawford et al.*, 2003], we can calculate CO_2 fluxes from the RR (1.2×10^9 mol/yr), CLSC (1.5×10^9 mol/yr), and NWLSC (4.3×10^9 mol/yr). Scaled to the 377 km total length of these three back-arc ridge segments, this represents a CO_2 flux per km of ridge that is similar to that estimated for depleted mid-ocean ridges [*Saal et al.*, 2002], suggesting that most of the CO_2 subducted beneath the Lau Basin is either delivered efficiently to Tonga arc volcanoes, or is subducted beyond the depths of back-arc magma generation.

6. Chalcophile Element Systematics During Low-Pressure Differentiation

6.1. Dry (MORB) Versus Wet (Manus Basin) Melts

[23] Nominally anhydrous MORB show a concomitant decrease in Cu and Ag (Figure 3) with decreasing MgO, attributable to sulfide melt removal during differentiation under sulfide-saturated conditions [*Mathez*, 1976; *Czamanske and Moore*, 1977; *Peach et al.*, 1990; *Doe*, 1995; *Yi et al.*, 2000; *Jenner et al.*, 2010]. The Se/S of MORB only subtly decreases with decreasing MgO (Figure 7a), whereas Cu/S, Cu/Se and Ag/Se (Figures 7b and 7c) are fractionated by sulfide removal; this is consequent to the lower partition coefficients of S and Se compared to Cu and Ag (Figure 7d) between sulfide melt and silicate melt [e.g., *Peach et al.*, 1990; *Stimac and Hickmott*, 1994]. Notably, Ag/Cu remains constant with decreasing MgO, demonstrating near identical sulfide-melt silicate-melt partition coefficients for Cu and Ag.

[24] In contrast to MORB, volcanic glasses from the Manus Basin record a muted increase in FeO_{TOT} and TiO_2 with decreasing MgO (Figure 3). Contrasting fractionation paths can be attributed to differences in the sequence of crystalline phase appearance on the liquidus of 'dry' MORB melts (olivine-plagioclase-clinopyroxene) compared to 'wet' subduction-related melts (olivine-clinopyroxene-Ca-rich plagioclase-amphibole), resulting in the evolution to typically higher SiO_2 contents of the latter [see *Arculus*, 2004], and the lower frequency in eruption of high MgO compositions. Between 9 and 3 wt.% MgO, samples from the Manus Basin show an increase in Se, Cu, and Ag and relatively constant Cu/Se, Ag/Se and Ag/Se with decreasing MgO, indicating these melts were sulfide-undersaturated [*Jenner et al.*, 2010]. The extremely low S contents and highly variable S/Se in Manus Basin samples with between 9 and 3 wt.% MgO (S/Se ranges from 291 to 639) indicate S was lost via degassing during eruption (Figure 3), complicating interpretations of the behavior of S during magma chamber processes. In addition to S loss, pervasive degassing of samples from the Manus Basin is evident from extremely low CO_2 contents (2.00–4.35 ppm; Table S3) and the high relative standard deviation (1σ) in replicate (3) analyses of both CO_2 (1–88%) and H_2O (0.8–12%). Fortuitously Se mimics the behavior of S during differentiation (Figure 3f), but unlike S (and other volatile elements such as CO_2), Se is not lost during degassing [*Jenner et al.*, 2010], likely linked to differences in redox systematics between S and Se; sulfur transitions from S^{2-} to S^{6+}, whereas Se transitions from Se^{2-} to Se^{4+} with increasing fO_2 [*Wykes et al.*, 2011]. Consequently, the measured content of Se ([Se]), in combination with an estimation of the initial S/Se of the melt prior to degassing, can be used to estimate the content of S (S*) in a melt prior to degassing and to constrain the behavior of S during differentiation in a crustal magma chamber prior to eruption [*Jenner et al.*, 2010]. Assuming a S/Se of between 3000 (approximate S/Se of primitive MORB), S* in the most primitive Manus Basin sample (MD3; [Se] = 0.131 ppm) is 392 ppm (open triangles on Figure 3). However, the mantle source region of the Manus Basin magmas is typically considered to be highly depleted [*Kamenetsky et al.*, 2001; *Sinton et al.*, 2003; *Jenner et al.*, 2010], consistent with the

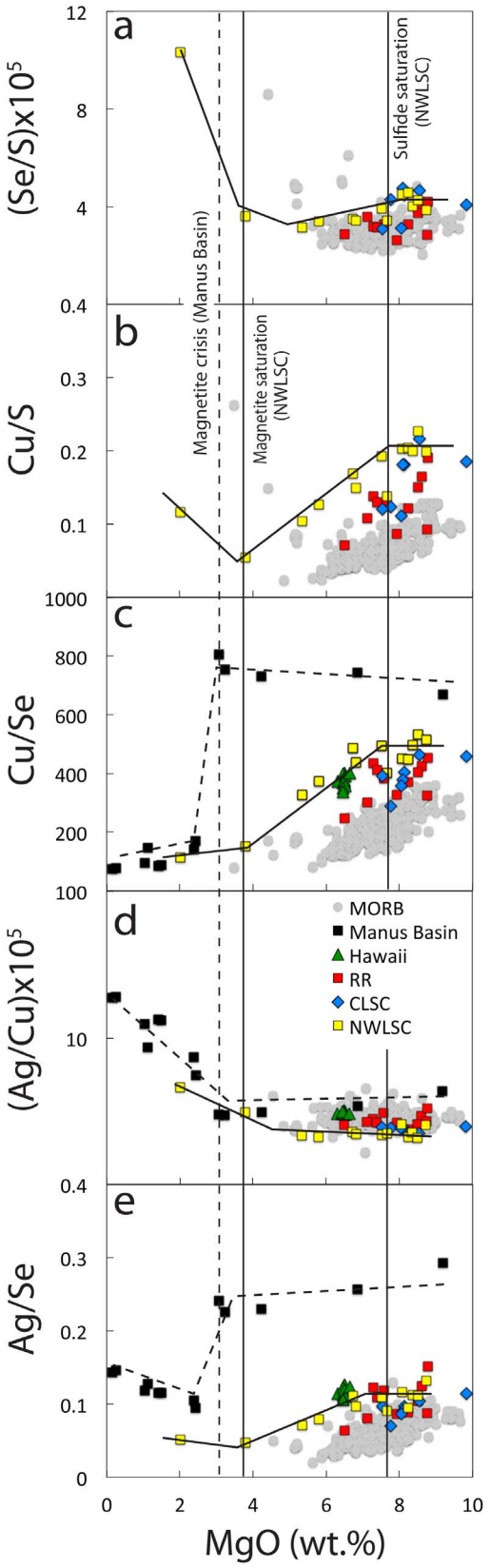

higher Cu/Se and Ag/Se of the most primitive samples from the Manus Basin compared to MORB (differences in the relative compatibility of the chalcohile elements in mantle sulfides (S < Se < Cu ≈ Ag) would result in an increase in Ag/Se, Cu/Se and decrease in S/Se with progressive depletion of the source [*Hamlyn et al.*, 1985; *Peach et al.*, 1990; *Stimac and Hickmott*, 1994; *Jenner et al.*, 2010]. Consequently, the initial S/Se of the Manus Basin magmas is likely to be substantially lower than MORB. Using a lower S/Se of 1800 [see *Jenner et al.*, 2010], S* of the most primitive Manus Basin sample is 235 ppm (open circles on Figure 3). Both estimates of S* indicate the primitive Manus Basin magmas would be sulfide undersaturated even if all the S in the melt was dissolved as S^{2-} (Figure 8a), and both estimates are substantially lower than the levels required to achieve S-saturation in relatively oxidized magmas [*Jugo et al.*, 2005].

[25] At ~3 wt.% MgO and with further decreases in MgO, the contents of Se, Cu, Ag and the Cu/Se and Ag/Se suddenly decrease, coincident with onset of magnetite-fractionation (Figures 3 and 7). This decrease was attributed by *Jenner et al.* [2010] to magnetite-triggered sulfide saturation (the 'Magnetite Crisis'), because a modest change in the

Figure 7. Variations in chalcophile element ratio versus MgO for samples from the NWLSC, RR, CLSC, Manus Basin, Hawaii and MORB. Inferred liquid lines of decent for the samples from the NWLSC and the Manus Basin (black lines) are given to highlight the trends discussed in the text. Sulfide-saturated MORB show a progressive decreasing in Se/S, Cu/S, Cu/Se and Ag/Se with decreasing MgO, which can be attributed to removal of sulfide melt during differentiation. Ag/Cu remains constant during sulfide melt fractionation from the melt. Prior to sulfide saturation for samples from the NWLSC (~7 wt.% MgO and prior to magnetite fractionation) and Manus Basin (~3 wt.% MgO and coinciding with magnetite saturation, referred to as the 'magnetite crisis' in *Jenner et al.* [2010]), chalcophile element contents remain constant because each of the chalcophile elements are equally incompatible in the evolving melt. Following sulfide saturation, samples from the NWLSC show a parallel change in chalcophile element ratios to those observed in MORB, indicating saturation in sulfide liquid (i.e., decrease in Cu/S, but constant Ag/Cu), whereas samples from the Manus basin show an increase in Ag/Cu, indicating saturation in a crystalline Cu-sulfide phase, such as bornite. Following magnetite fractionation, the Se/S, Cu/S and Ag/Cu of the NWLSC magmas increase, indicating a change in the nature of the sulfide phase on the liquidus from sulfide liquid to a crystalline Cu-sulfide phase.

Fe redox ratio of the melt, resulting from magnetite fractionation, has a dramatic effect on sulfur speciation; the dissolved S in the melt switches from mostly sulfate to sulfide, forcing the appearance of sulfide on the liquidus. Prior to the Magnetite Crisis, [Se] = 0.360 ppm (average of samples MD7a and MD7b), indicating an increase in the S content of the melt from 235 ppm in the most primitive sample to 648 ppm (assuming a S/Se of 1800), complemented by an increase in the contents of Cu and Ag from 88 to 281 ppm, and from 0.038 to 0.084 ppm, respectively. *Jenner et al.* [2010] used the change in Ag/Cu following the Magnetite Crisis, which is not observed in MORB (Figure 7d), to suggest saturation in a crystalline Cu-rich sulfide phase, such as bornite, at this stage in the evolution of the Manus Basin melts, as opposed to the removal of sulfide melt during the differentiation of MORB melts. Hence, the drop in [Se] resulting from sulfide saturation (Δ[Se] = 0.160 ppm; calculated between samples MD7 and MD8) and the S/Se of bornite (S/Se of 904, from the average of four analyses of Cu rich sulfide from *Core et al.* [2006]) can be used to estimate the complementary drop in S (Δ[S*]) following sulfide saturation to be 145 ppm (Δ[S*] = Δ[Se] $\times$ $(S/Se)^{bornite}$; see *Jenner et al.* [2010] for further discussion). Hence, S* in the melt following the 'Magnetite Crisis' is 503 ppm (slight differences in the estimations of S* presented here for the Manus suite compared to those presented in *Jenner et al.* [2010], result from improvements in LA-ICP-MS analytical techniques described in detail in *Jenner and O'Neill* [2012b].

[26] Using a S/Se of 1800 for the parental melt, [S*] calculated both prior to and following the Magnetite Crisis (648 and 503 ppm, respectively) plot below the S-saturated MORB array (open and black circles; Figure 8a). However, because the melts evolved to high Cu contents prior to sulfide

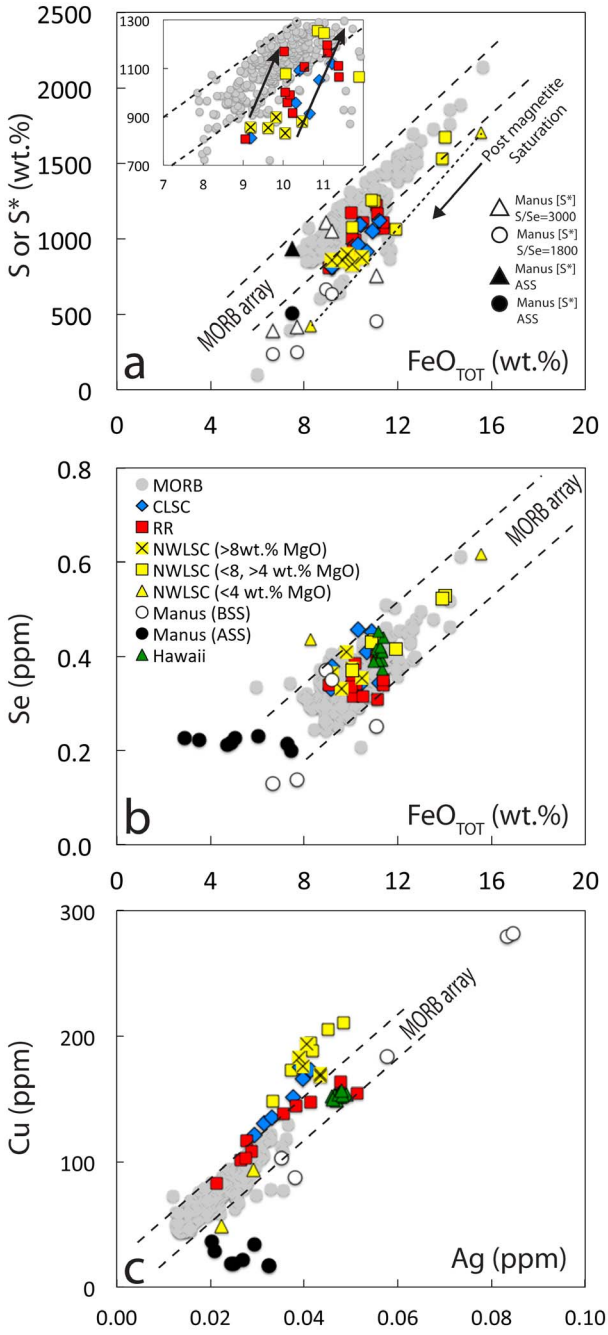

Figure 8. Variations in (a) S or S*, (b) Se versus FeO_{TOT} and (c) Cu versus Ag for samples from the NWLSC, RR, CLSC, Manus Basin and Hawaii compared to MORB (ASS = after sulfide saturation, BSS = before sulfide saturation). Inset on Figure 8a of S versus FeO_{TOT} more clearly demonstrates the low S contents of primitive (>8. wt.% MgO) samples from the NWLSC compared to the MORB array, indicating melts were initially S-undersaturated. Additionally, the trend in compositions with increasing FeO_{TOT} and decreasing MgO (see arrows, Figure 8a inset) shows the samples with <8 wt.% MgO (sulfide saturated) plot within the MORB array. Following saturation in magnetite, the contents of S and FeO_{TOT} decrease and samples plot below the MORB array, indicating a decrease in the sulfur content at sulfide saturation (SCSS) following magnetite fractionation compared to MORB. Figure 8b shows the behavior of Se mirrors that of S supporting the use of Se as a proxy for S [*Jenner et al.*, 2010] in degassed melts and Figure 8c shows the contents of both Cu and Ag, and the Cu/Ag in samples from the NWLSC and CLSC are higher than the MORB array, indicating that their petrogenesis was different form MORB. The samples from the RR show higher Ag at a given Cu compared to samples from the NWLSC and CLSC and are more comparable to those from Hawaii.

saturation, the compositions of the Manus Basin magmas at sulfide saturation plot within the Cu-rich, Ni poor, S-saturated melt array [*Ripley et al.*, 2002; *Jenner et al.*, 2010, Figure 8], indicating saturation in a Cu-rich sulfide phase was likely. Using the MORB S/Se of 3000 does give a S* prior to sulfide saturation that plots within the MORB S-saturated array (open triangles, Figure 8a). However, as explained above, it is likely that the S/Se of the parental melt of the Manus suite was substantially lower than MORB, indicating a S/Se value of 3000 is too high. To fully exploit the use of S* for tracking the behavior of S in degassed magmas, and in particular, for estimating the initial contents of S in mantle-derived melts, a systematic -study of the variations in S/Se of a melt with varying pressures, degrees of mantle depletion and a range in fO_2 is required.

6.2. Low-pressure Fractionation of Chalcophile Elements in the NWLSC Magmas Prior to Magnetite Fractionation

[27] Despite the overall spread in La/Sm, Th/Yb, and Nb/Yb, the most primitive samples from the NWLSC have a relatively limited range in major and minor element compositions (Figure 3). Additionally, samples from along the length of the NWLSC converge on a coherent fractionation path indicative of predominantly low-pressure fractional crystallization prior to eruption, from parental melts with similar major element compositions. In contrast to samples from the NWLSC, samples from the CLSC and RR have a larger range in major and minor element compositions at a given MgO content, and less well-defined fractionation trends, indicating the parental melt compositions were more variable. In particular, the CLSC and the RR have a large range in Cu and Ag contents that span the region between the NWLSC samples and the MORB array. Accordingly, here we focus on the better-defined low-pressure fractionation trend of the NWLSC suite that spans a larger range in MgO contents compared to the CLSC and RR.

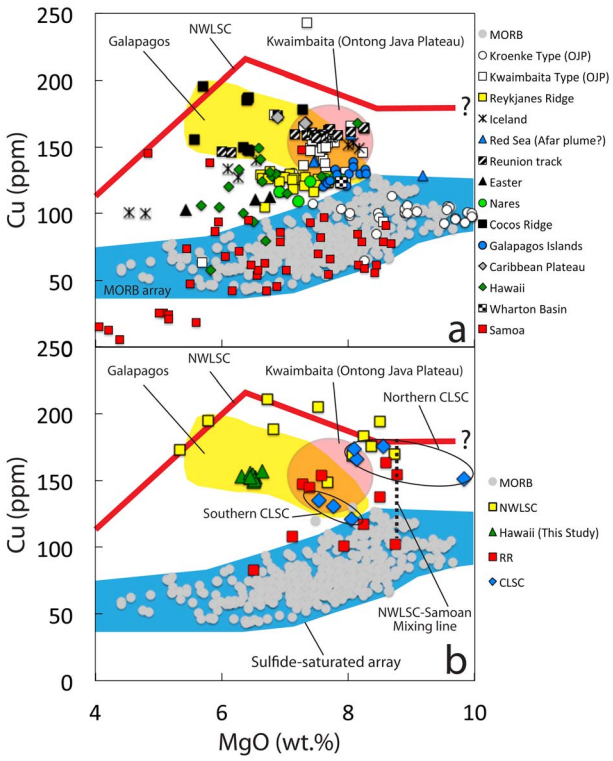

Figure 9. (a) Comparison of Cu versus MgO data for samples from the NWLSC, RR, Manus Basin and Hawaii compared to a compilation of previously published data. Figure 9a data sources: MORB, Reykjanes Ridge, Red Sea, Réunion hot spot track, Cocos Ridge, Easter island hot spot track, Nares Abyssal plain, Wharton Basin and Caribbean Plateau from *Jenner and O'Neill* [2012a]; Kroenke and Kwaimbaita Type OJP basalts [*Fitton and Godard*, 2004], Hawaii [*Norman et al.*, 2004], Iceland [*Hansen and Grönvold*, 2000; *Flude et al.*, 2010], Galapágos [*Harpp et al.*, 2003], Samoa [*Workman et al.*, 2004; *Jackson et al.*, 2010]. The majority of these sample localities have previously been linked to plume related magmatism: the Chagos-Laccadive Ridge, considered part of the Réunion hot spot track [e.g., *Fisk et al.*, 1989]; the Cocos Ridge of the Galapágos hot spot track [e.g., *O'Connor et al.*, 2007]; the Reykjanes Ridge, south of Iceland [*Hilton et al.*, 2000]; the Wharton Basin (Deep Sea Drilling Project (DSDP) Site 213), which are isotopically comparable to samples from the Kerguelen Plume [*Weis and Frey*, 1996]; core samples from the Caribbean Sea (Leg 15 Site 150 of the DSDP) [*Donnelly et al.*, 1973], considered part of the Caribbean Plateau [see *Geldmacher et al.*, 2003]; the Red Sea, which can likely be linked to the Afar plume-related magmatism [*Barrat et al.*, 1993]. Red line shows the inferred liquid line of descent for samples from the NWLSC and the likely composition of the parental magma (shown as '?'). Blue shaded field shows the MORB S-saturated array. Unlike the majority of plume-related melts, samples from the Samoan islands plot within the MORB, low-Cu, S-saturated array, indicating that they were saturated in sulfide during low-pressure differentiation. (b) Primitive samples from the RR plot on a mixing line (dashed black line) between the high-Cu melts of the NWLSC and low-Cu melts of the Samoan plume. Samples from the northern parts of the CLSC show elevated Cu contents at a given MgO, comparable to the NWLSC magmas, indicating their parental magmas were generated by melting at higher pressures compared to MORB, resulting in S-undersaturated melts following ascent through the mantle to lower pressures.

[28] The trends in major element contents with decreasing MgO of the NWLSC suite are more comparable to nominally anhydrous MORB than the Manus Basin suite (Figure 3). FeO_{TOT}, TiO_2, V, and Re contents of NWLSC samples show an initial increase with decreasing MgO until ~5 wt.% MgO, followed by a decrease in abundances with further differentiation, attributable to the appearance of magnetite on the liquidus (Figure 3). The complementary decrease in Re at the onset of magnetite saturation in samples from both the Manus Basin and NWLSC supports the conclusion of *Jenner et al.* [2010] that Re is magnetite-compatible during low-pressure differentiation.

[29] The contents of S and Se in primitive samples from the NWLSC are comparable to MORB and both elements mimic the behavior of FeO_{TOT} during differentiation (Figures 3e and 3f). Unlike samples from the Manus Basin, and Hawaiian subaerially erupted magmas, samples from the NWLSC (plus CLSC and RR) show no evidence for S-loss during eruption. In contrast to S and Se, initial contents of Cu, Ag, and Re in NWLSC glasses are substantially higher than MORB. Further, unlike MORB, Cu and Ag initially increase until ~7 wt.% MgO, at which stage contents of both elements decrease with further differentiation of the melts. The initial increase in Cu and Ag and the approximately constant Se/S, Cu/S, Cu/Se, and Ag/Se of samples from the NWLSC (Figure 7) indicates the parental melts were sulfide-undersaturated, similar to the Manus Basin. This conclusion is supported by consistently lower contents of S (~100–200 ppm) at a given FeO_{TOT} of NWLSC samples with >8 wt.% MgO compared to the sulfide-saturated MORB array (Figure 8a inset). The contents of Cu and Ag in samples from the NWLSC decrease with decreasing MgO in samples with <7 wt.%, indicating saturation in a sulfide phase was achieved by ~7 wt.% MgO. This interpretation is supported by changes in Se/S, Cu/S, Cu/Se and Ag/Se at this stage in melt evolution. Notably, the Ag/Cu of samples with between 4 and 7 wt.% MgO remains constant, and Se/S, Cu/S, Cu/Se and Ag/Se decrease at a comparable rate to MORB, indicating removal of sulfide melt as opposed to a crystalline sulfide phase during early stages of differentiation of the melt (Figure 7). The content of Re continues to increase regardless of the decrease in Cu and Ag (Figure 3d), demonstrating Re is not compatible in the fractionating sulfide melt.

[30] The change in partitioning behavior of Cu and Ag coincides with the liquid line of descent for S versus FeO_{TOT} moving into the MORB sulfide-saturated array (evolution of the NWLSC melt shown by arrows on Figure 8a inset), demonstrating the higher bulk partition coefficient of FeO_{TOT} compared to S prior to sulfide saturation. Unlike samples from the Manus Basin, sulfide saturation in samples from the NWLSC (~7 wt.% MgO) is achieved prior to the onset of magnetite fractionation (~5 wt.% MgO; Figure 3). Hence, magnetite-triggered-reduction of the evolving magma was not required to trigger sulfide saturation; i.e., the primitive melts generated in the NWLSC were less oxidized than samples from the Manus Basin and more similar to MORB.

[31] Unlike Cu and Ag, the content of S in samples from the NWLSC continues to increase between 7 wt.% MgO and ~5 wt.% MgO (Figure 3e), because the solubility of S is predominantly controlled by the proportion of FeO_{TOT} [*O'Neill and Mavrogenes*, 2002], with the net surplus of S relative to FeO_{TOT} during differentiation removed by sulfide precipitation. Similarly, the content of Se also increases between 7 and 5 wt.% MgO (Figure 3f), which can likely be attributed to Se occupying the same site in the melt structure as S (i.e., the sulfur content at sulfide saturation (SCSS) is actually the sum of S+Se), resulting in the relatively constant, or subtle decrease in Se/S of MORB and the NWLSC samples with between 7 and 5 wt.% MgO; Figure 7). Hence, Cu and Ag are more useful for pinpointing the onset of sulfide saturation than S and Se.

6.3. Low-pressure Fractionation of Chalcophile Elements in the NWLSC Magmas After Magnetite Fractionation

[32] Curiously, the most evolved NWLSC samples (<4 wt.% MgO; Figure 8a) plot on a trend between S and FeO_{TOT} at an angle and slightly below the field for sulfide-saturated MORB, indicating a drop in the SCSS compared to the MORB array. This drop in S contents at a given FeO_{TOT} coincides with the onset of magnetite fractionation and the sudden increase in the Se/S, Cu/S, and Ag/Cu of erupted melt. The relative change in behavior of S, Se, Cu, and Ag at the onset of magnetite saturation, in particular Ag/Cu, which remains constant during the evolution of MORB melts, indicates a change in the composition of the sulfide phase (previously sulfide liquid) on the liquidus (Figure 7). This apparent drop in the SCSS may in turn be linked to reduction of the melt associated with the removal of magnetite. An increase in Ag/Cu is also observed

in samples from the Manus Basin, following magnetite-triggered sulfide saturation, which *Jenner et al.* [2010] attributed to the appearance of a crystalline Cu-rich sulfide phase on the liquidus, such as bornite, as opposed to sulfide liquid. It is conceivable that magnetite saturation coupled with a decrease in temperature during continued differentiation in a crustal magma chamber, results in a change in phase composition on the liquidus of the NWLSC magmas from sulfide liquid, to a more Cu-rich composition. Alternatively, the increased compatibility of Cu relative to Ag at this stage in the fractionation sequence may indicate that Cu is slightly compatible in magnetite. However, the systematic changes in each of the chalcophile element ratios, including S and Se, which are unlikely to partition into magnetite, supports our conclusion that there is a change in the composition of the fractionating sulfide, potentially from a liquid to a crystalline sulfide phase with a stoichiometry capable of fractionating Cu from Ag.

7. Origin of Sulfide-Undersaturated Melts

[33] *Jenner and O'Neill* [2012a] used Cu versus MgO to demonstrate submarine-quenched samples erupted along known hot spot tracks or close to areas associated with plume-related magmatism have higher Cu contents at a given MgO compared to the typical MORB array (compilation shown on Figure 9). Similarly, our data for Hawaii (Pu'u'O'o eruption of Kilauea), and compiled data from Ko'oalau and Moloka'i Hawaiian volcanoes, Iceland, Kwaimbaita-Type magmas from the Ontong Java Plateau and the Galápagos Islands have high Cu at a given MgO compared to the MORB array, indicating elevated Cu contents is a common characteristic of magmas associated with mantle plumes. The only samples presented in Figure 9 that are generated by plume-related magmatism but do not have higher Cu contents compared to the MORB array are the primitive Kroenke-type magmas from the Ontong Java Plateau, and conspicuously, samples from the Samoan islands. The most straightforward explanation for the higher Cu contents at a given MgO of the majority of plume-related samples compared to MORB, is the parental melts, like the NWLSC magmas, were initially S-undersaturated and consequently, evolved to high Cu contents compared to sulfide-saturated MORB. The high Cu contents of the more evolved Kwaimbaita-type basalts indicate the Ontong Java Plateau melts were indeed S-undersaturated during differentiation (considered by *Fitton and Godard* [2004] to be linked to the Kroenke-type magmas by fractional crystallization), consistent with conclusions of other studies [*Ely and Neal*, 2003; *Chazey and Neal*, 2004]. Hence, some part of the petrogenesis of parental magmas of each of these Cu-rich melts discussed above was likely similar to that of NWLSC samples consequent to parental magmas being S-undersaturated.

[34] S-undersaturated melts could be generated by high-degrees of partial melting if the sulfide phase in the mantle source region became exhausted. For example, komatiites-komatiitic basalts were S-undersaturated during low-pressure fractional crystallization [*Puchtel and Humayun*, 2000, 2001]. However, the most primitive samples retrieved from the NWLSC, RR and CLSC all have MgO contents <10 wt.%, indicating these were not high-degree partial melts. Additionally, samples from the NWLSC, RR and CLSC have REE patterns similar to MORB (Figure 4c) and plot within the MORB array with regards to Th/Yb versus Nb/Yb (Figure 5), indicating similar degrees of partial melting. Given the melt-depleted upper mantle sources of MORB are generally considered to contain residual sulfides [*Peach et al.*, 1990], we can infer sulfide was also present in the mantle source region of these northwestern Lau Basin magmas.

[35] Experimental studies have demonstrated SCSS decreases with increasing pressure [*Mavrogenes and O'Neill*, 1999]. During adiabatic upwelling of a melt, S-saturated melts generated at high pressures will be S-undersaturated at lower pressures. For example, using the experimental constraints presented in *Mavrogenes and O'Neill* [1999] for basaltic compositions, a melt with a temperature of 1200°C and 10 wt.% FeO_{TOT}, the SCSS at 1.2 GPa is 750 ppm, at 0.9 GPa is 850 ppm, and at 0.3 GPa is 950 ppm. Given the parental magmas of the NWLSC have ~100–200 ppm less S at a given FeO_{TOT} compared to the MORB array (Figure 8), we suggest the former were generated at pressures at least ~0.6–0.9 GPa higher than typical MORB, but at pressures lower than garnet stability (~2.8 GPa [*Robinson and Wood*, 1998]) to prevent the fractionation of the HREE. Although in detail subtle differences in the composition of the parental melt, such as Cu content, also affects the SCSS [*O'Neill and Mavrogenes*, 2002; *Ripley et al.*, 2002], these variables do not result in the production of S-undersaturated parental melts.

[36] Subsequent to partial melting, retention of higher-pressure (S-saturated) lower S contents compared to MORB, requires NWLSC parental magmas to have ascended rapidly, i.e., without equilibrating with surrounding mantle during ascent and maintaining S-saturation, resulting in parental melts that were S-undersaturated during initial stages of low-pressure fractional crystallization. This interpretation is supported by the geographic locations of the high-Cu samples plotted on Figure 9; each of the samples were erupted at locations linked to plume-related magmatism. Hence, we consider the S-undersaturated signatures of samples from the NWLSC and parts of the CLSC and RR, indicates the generation of the parental melts was more comparable to the petrogenesis of plume-related magmas as opposed to MORB, but at pressures less than the garnet stability field.

[37] Geophysical studies, including bathymetric and seismic constraints coupled with numerical modeling, have attributed the anomalously high topography of a region spanning the North Fiji Basin, North Fijian Plateau and northern Lau Basin to the upwelling of hot, buoyant mantle [*Billen and Gurnis*, 2003; *Zhang and Pysklywec*, 2006]. The presence of deep mantle upwelling(s) may account for the geochemical characteristics of the Northwest Lau Basin we have identified herein. An extremely high incidence of hydrothermal activity reported in this part of the Lau Basin [*Lupton et al.*, 2012b], also indicates the area is anomalously hot. Although samples from the NWLSC lack the characteristic high-pressure garnet signature (i.e., high Gd/Yb_{PM}) typical of plume-related melts such as Hawaii and Samoa, this may not preclude the magmatism in the NWLSC being linked to a 'deep' upwelling of the mantle. For example, the physical upwelling resulting in the production of the NWLSC melts may have been present in the garnet stability field, but derived melts will only record high Gd/Yb_{PM} if the solidus was intersected at this depth. It is worth noting the petrogenesis of oceanic plateau basalts, (e.g., Ontong Java) which have Gd/Yb, Th/Yb, and Nb/Yb similar to the NWLSC (Figures 4 and 5), is typically linked to plume-related magmatism, but these samples also lack a garnet control signature [*Fitton and Godard*, 2004].

[38] The compilation presented in Figure 9 shows a number of Samoan islands samples are S-saturated (i.e., the contents of Cu decrease with decreasing MgO), and plot almost entirely within the MORB array. This interpretation is supported by the occurrence of sulfides in the majority of submarine alkali basaltic glasses from the three youngest Samoan volcanoes, Ta'u, Malumalu and Vailulu'u [*Workman et al.*, 2006]. The cause of the S-saturated characteristics of the magmas sourced by the Samoan plume, which contrasts with the S-undersaturated nature of the majority of plume-derived melts compiled in Figure 9 is enigmatic, and beyond the scope of this contribution, but may be linked to their more alkali-rich compositions or magma ascent rates.

8. High Cu Contents in Samples from the Northwest Lau Basin

[39] The most primitive samples from the NWLSC and a number of samples from the RR and CLSC have the highest Cu contents of all of the samples compiled in Figure 9, implying either: (1) the parental melts were generated by high-degrees of partial melting, producing high-Mg parental melts that evolved to high Cu contents during extensive sulfide-undersaturated differentiation; or (2), the partial melts are anomalously rich in Cu. Th/Yb versus Nb/Yb systematics and the PM- normalized patterns of samples from the CLSC, NWLSC, and RR show no evidence for a subduction-derived input to the mantle source region of the NWLSC samples (Figures 4 and 5). Hence, it is unlikely that the high Cu and Ag contents resulted from subduction-related processes. Additionally, the contents of Cu, Ag, and Se in primitive samples from the Manus Basin plot either within or below the MORB array, despite the trace element evidence for a subduction component to their mantle source region, indicating minimal mobility of these elements compared to elements such as As, Sb, Tl, Bi and Pb.

[40] *Fitton and Godard* [2004] demonstrated the range in major and trace element compositions of primitive Kroenke-type magmas from the Ontong Java Plateau can be generated by olivine-only fractionation. Additionally, *Fitton and Godard* [2004, Figure 10] used the range in Nb versus MgO contents to demonstrate the more pronounced enrichment of incompatible elements after the appearance of plagioclase and clinopyroxene on the liquidus, and the ability of fractional crystallization to generate the differences in compositions of the primitive Kroenke-type and the more evolved Kwaimbaita-type magmas. Olivine ± chromite are typically the only phases on the liquidus of melts with >8 wt. MgO [e.g., *Langmuir et al.*, 1992]. The

approximately constant Cu contents with decreasing MgO of the Kroenke-type magmas (Figure 9a), demonstrates olivine ± chromite only fractionation is unable to generate the high-Cu contents of the most mafic NWLSC basalts from a picritic, low-Cu parental melt composition. Accordingly, the red line on Figure 9 indicates the likely Cu content of any parental NWLSC magmas at higher MgO contents. Thus we consider the high Cu contents of the NWLSC magmas and a number of samples from the RR and CLSC to be a diagnostic feature of the parental melts.

[41] In addition to the high Cu and Ag contents of the most primitive NWLSC samples and a number of samples from the CLSC and RR, the initially high Cu/Se, Cu/S, and Ag/S are distinctive. With progressive depletion of the mantle source region, the Cu/S, Cu/Se and Ag/Se of subsequent melts are expected to increase because of the higher compatibility of Cu and Ag in the residual mantle sulfide compared to both S and Se [*Hamlyn et al.*, 1985; *Peach et al.*, 1990; *Jenner et al.*, 2010]. Given NWLSC have LREE compositions that plot within the range of MORB and are not markedly depleted, the Cu/S, Cu/Se and Ag/Se are expected to plot within the MORB array and not substantially above it. Similarly, other plume-related suites, such as the Hawaiian basalts (Figure 7), samples from the Réunion hot spot track and Cocos Ridge also have high Cu/Ag and Ag/Se compared to the MORB array. This behavior contrasts with the predicted chalcophile element behavior of samples from the Manus Basin (Figure 7) and data for boninites [*Hamlyn et al.*, 1985], which are considered to have been derived from extremely depleted mantle source regions [*Hamlyn et al.*, 1985; *Kamenetsky et al.*, 2001; *Sinton et al.*, 2003; *Jenner et al.*, 2010] and in accord with our understanding of chalcophile element systematics, have elevated Cu/Se and Ag/Se compared to less depleted MORB. Hence, the high Cu and Ag contents of samples from the NWLSC and some samples from the CLSC and RR, and the high Cu/S, Cu/Se and Ag/Se appear to be diagnostic features resulting from the petrogenesis of the parental magmas.

[42] *Urakawa et al.* [1987] showed the eutectic in the Fe-Ni-O-S system remains below 900°C to 15 GPa, indicating sulfides are molten throughout the mantle. Consequently, it is difficult to envisage why partitioning behavior would change with depth, or permit the production of variably Cu-rich parental melts. Alternatively, other experimental studies found that two sulfide phases are stable in the upper mantle, a crystalline Fe-S-rich monosulfide and a Cu-Ni enriched sulfide melt [*Bockrath et al.*, 2004; *Ballhaus et al.*, 2006]. These studies concluded that during melt segregation, monosulfide stays in the residual solid residue whereas the Cu-rich sulfide melt is entrained as immiscible droplets in the silicate melt, providing a means to fractionate the chalcophile and siderophile elements from each other during melting, as observed in the Lau Basin samples. Sulfide liquids are not quenchable to glass, even in rapidly quenched experiments, and instead crystallize on cooling to a variably complex phase assemblage depending on their exact composition, making interpretation of their results challenging. The two-phase field of monosulfide plus sulfide melt derived from textural relationships could merely be a quench texture. However, we note models presented by *Bockrath et al.* [2006] and *Ballhaus et al.* [2006] are able to reproduce the PGE fractionated patterns of silicate melts. Alternatively, *Ripley et al.* [2002] used sulfide liquid/silicate partition coefficients in experimental runs to demonstrate an increase in Cu solubility in the silicate melt with moderate increases in fO_2. Hence, parental melts of the NWLSC basalts may have been slightly more oxidised than MORB, but not oxidized enough to prevent saturation in sulfide during differentiation of the melts at low pressure, and notably with regards to the differentiation of backarc basin magmas, before the Magnetite Crisis. Quantitatively resolving the cause of the initially high Cu contents of the NWLSC magmas and plume-related melts is beyond the scope of this contribution and likely requires further experimental studies regarding the partitioning of chalcophile elements at high pressure.

9. The use of Cu for Tracking the Ingress of the Samoan Plume

[43] We attribute the S-undersaturated compositions of the most primitive samples from the NWLSC and a number of samples along the RR and CLSC to partial melting at pressures greater than MORB. Previous studies have attributed a range of geochemical proxies in samples from the northern part of the Lau Basin to lateral entrainment of material from the Samoan Plume into and mixing with the local mantle [*Lupton and Craig*, 1975; *Volpe et al.*, 1988; *Poreda and Craig*, 1992; *Turner and Hawkesworth*, 1998; *Falloon et al.*, 2007; *Regelous et al.*, 2008; *Lupton et al.*, 2009; *Tian et al.*, 2011; *Hahm et al.*, 2012; *Lupton et al.*,

2012a]. However, samples from Samoa plot almost exclusively within the MORB array on the plot of Cu versus MgO (Figure 9). Consequently the high Cu and Ag contents of the NWLSC are not easily attributable to ingress of the Samoan plume and in particular, mixing between two low-Cu sources, such as Samoan and MORB. We suggest the RR result from the mixing of two distinct end-member compositions; (1) a high-Cu, relatively high $^3He/^4He$ (~20) component beneath the NWLSC generated at pressures higher than MORB; (2) a low-Cu, Samoan plume ($^3He/^4He$ ~30) component invading beneath the RR (see mixing line on Figure 9b). Additionally, we note that the offset to higher Ag at a given Cu content of samples from the RR compared to both the NWLSC and CLSC is a feature shared by OIB samples from Hawaii (Figure 8c), indicating the Samoan plume material may share this characteristic. This interpretation is also supported by the subtly higher Gd/Yb, TiO_2 and lower V of the RR samples compared to those generated at the NWLSC, which is consistent with some extent of mixing with a Samoan-plume component. The ingress of Samoan material into the Northern Lau Basin (red arrow, Figure 1b) is likely facilitated by toroidal flow of the mantle around the northern limit of the Pacific Slab during rapid migration of the trench [*Schellart*, 2004; *Stegman et al.*, 2006; *Schellart et al.*, 2007].

[44] The presence of the Pacific Slab beneath the CLSC (~300 km) possibly prevents the high-Cu signals in the northern parts of this spreading center being derived from a Transition Zone or a lower mantle-derived plume. Additionally, the consistently low $^3He/^4He$ of ~8 of both the high-Cu and low-Cu melts from the CLSC indicates mixing between the high $^3He/^4He$ NWLSC and MORB-like source cannot be invoked to explain the geochemical compositions of the CLSC magmas. The high Cu contents of some of the samples from the CLSC indicates the parental magmas were generated by melting at higher pressures than MORB, lending support for models that have suggested the existence of subduction-triggered plume-like mantle upwellings in backarc basin regions [e.g., *Faccenna et al.*, 2010]. Similarly, the high Cu contents of samples from the NWLSC, which are comparable in magnitude to those generated in the CLSC, may indicate poloidal flow of material from beneath and around the edges of the flat-lying section of the Pacific Plate (yellow arrow, Figure 1b; the angle of subduction of the Pacific Plate shallows between ~300–400 km, at a distance of ~400–600 km from the Tonga Trench [*Richards et al.*, 2011]) may have triggered upwelling of the mantle to produce the NWLSC magmas.

10. High Pb, Tl and As Signatures of the RR Magmas: The Remnant Vitiaz Arc?

[45] A notable feature of the RR samples are enrichments in Pb, As, and especially Tl on PM-normalized plots, compared to MORB and samples from the NWLSC and the CLSC (Figure 4). These distinctively high Pb, As, and Tl patterns may indicate the Samoan OIB magmas are also enriched in these elements, although to the best of our knowledge, relevant data are currently unavailable to test this hypothesis. However, we note there is no correlation between the magnitude of the Pb, As, and Tl anomalies with other indicators of mixing with the Samoan component, such as Gd/Yb, V, TiO_2 or the chalcophile elements. The enrichments in Pb, As, and Tl in samples from the RR are comparable to subduction-related samples from the Manus Basin, but the magnitude in the Tl enrichment compared to Pb, As, and Mo indicates differences in their petrogenesis. Additionally, samples from the RR lack other commonly recognized geochemical characteristics of subduction-related magmatism, such as depletions in Nb and Ta relative to La, enrichments in Cs relative to Rb, or elevated Th/Yb at a given Nb/Yb. In addition to Tl anomalies, samples from the RR have negative Y depletions relative to Ho on primitive mantle plots, which are not observed in samples from the NWLSC, the CLSC, the Manus Basin or samples defining the MORB array. Y and Ho are typically regarded as 'geochemical twins' and as such, are difficult to fractionate from each other during igneous processes [e.g., *Blundy and Wood*, 2003; *Pack et al.*, 2007]. However, hydrothermal alteration of oceanic crust, at temperatures between 100 and 400°C is capable of fractionating Y from Ho, as a result of chemical complexation and differences in electronic configuration between the two elements [*Bau*, 1996, and references therein]. Noting the basement of the RR may represent disrupted portions of the fossil Vitiaz Arc (Figure 1), we suggest the positive As, Tl and Mo anomalies and negative Y anomalies relative to Ho in the majority of samples from the RR may have resulted from variable assimilation of hydrothermally altered portions of this basement.

Acknowledgments

[46] We thank the officers, crew, and co-scientific staff of the SS07/2008 voyage for their professionalism and enthusiasm

that ensured the success of the expedition. The post-voyage analytical costs were supported by an Australian Research Council Discovery Grant to RJA and JM. Erik Hauri acknowledges funding from the Deep Carbon Observatory. Rick Carlson provided sagacious advice ré content and balance of an early draft of this paper, and we thank Jianhua Wang for expert maintenance and assistance in the DTM SIMS lab. Jon Blundy and Andreas Audétat are thanked for their constructive and thoughtful reviews and Joel Baker for editorial handling.

References

Arculus, R. J. (2004), Evolution of arc magmas and their volatiles, in *The State of the Planet: Frontiers and Challenges in Geophysics*, *Geophys. Monogr. Ser.*, vol. 150, edited by R. S. J. Sparks and C. J. Hawkesworth, pp. 95–108, AGU, Washington, D. C., doi:10.1029/150GM09.

Ballhaus, C., C. Bockrath, C. Wohlgemuth-Ueberwasser, V. Laurenz, and J. Berndt (2006), Fractionation of the noble metals by physical processes, *Contrib. Mineral. Petrol.*, *152*(6), 667–684, doi:10.1007/s00410-006-0126-z.

Barrat, J.-A., B. M. Jahn, S. Fourcade, and J. L. Joron (1993), Magma genesis in an ongoing rifting zone: The Tadjoura Gulf (Afar area), *Geochim. Cosmochim. Acta*, *57*(10), 2291–2302, doi:10.1016/0016-7037(93)90570-M.

Bau, M. (1996), Controls on the fractionation of isovalent trace elements in magmatic and aqueous systems: Evidence from Y/Ho, Zr/Hf, and lanthanide tetrad effect, *Contrib. Mineral. Petrol.*, *123*, 323–333, doi:10.1007/s004100050159.

Benz, H. M., M. Herman, A. C. Tarr, K. P. Furlong, G. P. Hayes, A. Villaseñor, R. L. Dart, and S. Rhea (2011), Seismicity of the Earth 1900–2010 eastern margin of the Australia plate, *U.S. Geol. Surv. Open File Rep.*, *2010-1083-I*.

Bevis, M., et al. (1995), Geodetic observations of very rapid convergence and back-arc extension at the Tonga arc, *Nature*, *374*, 249–251, doi:10.1038/374249a0.

Billen, M. I., and M. Gurnis (2003), Comparison of dynamic flow models for the Central Aleutian and Tonga-Kermadec subduction zones, *Geochem. Geophys. Geosyst.*, *4*(4), 1035, doi:10.1029/2001GC000295.

Blundy, J., and B. Wood (2003), Partitioning of trace elements between crystals and melts, *Earth Planet. Sci. Lett.*, *210*(3–4), 383–397, doi:10.1016/S0012-821X(03)00129-8.

Bockrath, C., C. Ballhaus, and A. Holzheid (2004), Fractionation of the platinum-group elements during mantle melting, *Science*, *305*(5692), 1951–1953, doi:10.1126/science.1100160.

Cartigny, P., F. Pineau, C. Aubaud, and M. Javoy (2008), Towards a consistent mantle carbon flux estimate: Insights from volatile systematics (H_2O/Ce, δD, CO_2/Nb) in the North Atlantic mantle (14°N and 34°N), *Earth Planet. Sci. Lett.*, *265*(3–4), 672–685, doi:10.1016/j.epsl.2007.11.011.

Chauvel, C., S. L. Goldstein, and A. W. Hofmann (1995), Hydration and dehydration of oceanic crust controls Pb evolution in the mantle, *Chem. Geol.*, *126*(1), 65–75, doi:10.1016/0009-2541(95)00103-3.

Chazey, W. J., and C. R. Neal (2004), Large igneous province magma petrogenesis from source to surface: Platinum-group element evidence from Ontong Java Plateau basalts recovered during ODP Legs 130 and 192, in *Origin and Evolution of the Ontong Java Plateau*, edited by J. G. Fitton et al., *Geol. Soc. Spec. Publ.*, *229*, 219–238, doi:10.1144/GSL.SP.2004.229.01.13.

Chen, C.-Y., F. A. Frey, M. O. Garcia, G. B. Dalrymple, and S. R. Hart (1991), The tholeiite to alkalic basalt transition at Haleakala Volcano, Maui, Hawaii, *Contrib. Mineral. Petrol.*, *106*(2), 183–200, doi:10.1007/BF00306433.

Cooper, L. B., D. M. Ruscitto, T. Plank, P. J. Wallace, E. M. Syracuse, and C. E. Manning (2012), Global variations in H_2O/Ce: 1. Slab surface temperatures beneath volcanic arcs, *Geochem. Geophys. Geosyst.*, *13*, Q03024, doi:10.1029/2011GC003902.

Core, D. P., S. E. Kesler, and E. J. Essene (2006), Unusually Cu-rich magmas associated with giant porphory copper deposits: Evidence from Bingham, *Utah Geol.*, *34*, 41–44, doi:10.1130/G21813.1.

Crawford, W. C., J. A. Hildebrand, L. M. Dorman, S. C. Webb, and D. A. Wiens (2003), Tonga Ridge and Lau Basin crustal structure from seismic refraction data, *J. Geophys. Res.*, *108*(B4), 2195, doi:10.1029/2001JB001435.

Czamanske, G. K., and J. G. Moore (1977), Composition and phase chemistry of sulfide globules in basalts from the Mid-Atlantic-Ridge rift valley near 37°N lat, *Geol. Soc. Am. Bull.*, *88*, 587–599, doi:10.1130/0016-7606(1977)88<587:CAPCOS>2.0.CO;2.

Doe, B. (1995), Zinc, copper, and lead geochemistry of oceanic igneous rocks—Ridges, islands, and arcs, *Int. Geol. Rev.*, *37*, 379–420, doi:10.1080/00206819509465410.

Donnelly, T. W., W. G. Melson, R. Kay, and J. J. W. Rogers (1973), Basalts and dolerites of Late Cretaceous age from the Central Caribbean, *Initial Rep. Deep Sea Drill. Proj.*, *15*, 989–1011, doi:10.2973/dsdp.proc.15.130.1973.

Dunkley, P. N. (1983), Volcanism and the evolution of the Ensimatic Solomon Islands Arc, in *Arc Volcanism: Physics and Tectonics*, edited by D. Shimozuru and I. Yokoyama, pp. 225–241, Terra Sci., Tokyo.

Ely, J. C., and C. R. Neal (2003), Using platinum-group elements to investigate the origin of the Ontong Java Plateau, SW Pacific, *Chem. Geol.*, *196*(1–4), 235–257, doi:10.1016/S0009-2541(02)00415-1.

Faccenna, C., T. W. Becker, S. Lallemand, Y. Lagabrielle, F. Funiciello, and C. Piromallo (2010), Subduction-triggered magmatic pulses: A new class of plumes?, *Earth Planet. Sci. Lett.*, *299*(1–2), 54–68, doi:10.1016/j.epsl.2010.08.012.

Falloon, T. J., L. V. Danyushevsky, T. J. Crawford, R. Maas, J. D. Woodhead, S. M. Eggins, S. H. Bloomer, D. J. Wright, S. K. Zlobin, and A. R. Stacey (2007), Multiple mantle plume components involved in the petrogenesis of subduction-related lavas from the northern termination of the Tonga Arc and northern Lau Basin: Evidence from the geochemistry of arc and backarc submarine volcanics, *Geochem. Geophys. Geosyst.*, *8*, Q09003, doi:10.1029/2007GC001619.

Fisk, M. R., R. A. Duncan, A. N. Baxter, J. D. Greenough, R. B. Hargraves, and Y. Tatsumi (1989), Reunion hotspot magma chemistry over the past 65 my: Results from Leg 115 of the Ocean Drilling Program, *Geology*, *17*(10), 934–937, doi:10.1130/0091-7613(1989)017<0934:RHMCOT>2.3.CO;2.

Fitton, J. G. (1995), Coupled molybdenum and niobium depletion in continental basalts, *Earth Planet. Sci. Lett.*, *136*(3–4), 715–721, doi:10.1016/0012-821X(95)00171-8.

Fitton, J. G., and M. Godard (2004), Origin and evolution of magmas on the Ontong Java Plateau, in *Origin and Evolution of the Ontong Java Plateau*, edited by J. G. Fitton et al., *Geol. Soc. Spec. Publ.*, *229*, 151–178, doi:10.1144/GSL.SP.2004.229.01.10.

Flude, S., D. McGarvie, R. Burgess, and A. Tindle (2010), Rhyolites at Kerlingarfjöll, Iceland: The evolution and

lifespan of silicic central volcanoes, *Bull. Volcanol.*, *72*(5), 523–538, doi:10.1007/s00445-010-0344-0.

Garcia, M. O., A. J. Pietruszka, J. M. Rhodes, and K. Swanson (2000), Magmatic processes during the prolonged Pu'u'O'o eruption of Kilauea Volcano, Hawaii, *J. Petrol.*, *41*, 967–990, doi:10.1093/petrology/41.7.967.

Geldmacher, J., B. B. Hanan, J. Blichert-Toft, K. Harpp, K. Hoernle, F. Hauff, R. Werner, and A. C. Kerr (2003), Hafnium isotopic variations in volcanic rocks from the Caribbean Large Igneous Province and Galápagos hot spot tracks, *Geochem. Geophys. Geosyst.*, *4*(7), 1062, doi:10.1029/2002GC000477.

Hahm, D., D. R. Hilton, P. R. Castillo, J. W. Hawkins, B. B. Hanan, and E. H. Hauri (2012), An overview of the volatile systematics of the Lau Basin–Resolving the effects of source variation, magmatic degassing and crustal contamination, *Geochim. Cosmochim. Acta*, *85*, 88–113, doi:10.1016/j.gca.2012.02.007.

Hall, R. (2001), Extension during late Neogene collision in east Indonesia and New Guinea, *J. Virtual Explorer*, *4*(4), 17–24, doi:10.3809/jvirtex.2001.00031.

Hamburger, M. W., and B. L. Isacks (1987), Deep earthquakes in the Southwest Pacific: A tectonic interpretation, *J. Geophys. Res.*, *92*(B13), 13,841–13,854, doi:10.1029/JB092iB13p13841.

Hamlyn, P. R., R. R. Keays, W. E. Cameron, A. J. Crawford, and H. M. Waldron (1985), Precious metals in low-Ti Lavas: Implications for metallogenesis and sulfur saturation in primary magmas, *Geochim. Cosmochim. Acta*, *49*(8), 1797–1811, doi:10.1016/0016-7037(85)90150-4.

Hannington, M., P. Herzig, S. Scott, G. Thompson, and P. Rona (1991), Comparative mineralogy and geochemistry of gold-bearing sulfide deposits on the mid-ocean ridges, *Mar. Geol.*, *101*(1–4), 217–248, doi:10.1016/0025-3227(91)90073-D.

Hansen, H., and K. Grönvold (2000), Plagioclase ultraphyric basalts in Iceland: The mush of the rift, *J. Volcanol. Geotherm. Res.*, *98*(1–4), 1–32, doi:10.1016/S0377-0273(99)00189-4.

Harpp, K. S., D. J. Fornari, D. J. Geist, and M. D. Kurz (2003), Genovesa Submarine Ridge: A manifestation of plume-ridge interaction in the northern Galápagos Islands, *Geochem. Geophys. Geosyst.*, *4*(9), 8511, doi:10.1029/2003GC000531.

Hart, S. R., E. H. Hauri, L. A. Oschmann, and J. A. Whitehead (1992), Mantle plumes and entrainment: Isotopic evidence, *Science*, *256*(5056), 517–520, doi:10.1126/science.256.5056.517.

Hart, S. R., M. Coetzee, R. K. Workman, J. Blusztajn, K. T. M. Johnson, J. M. Sinton, B. Steinberger, and J. W. Hawkins (2004), Genesis of the Western Samoa seamount province: Age, geochemical fingerprint and tectonics, *Earth Planet. Sci. Lett.*, *227*(1–2), 37–56, doi:10.1016/j.epsl.2004.08.005.

Hattori, K. H., S. Arai, and D. B. Clarke (2002), Selenium, tellurium, arsenic and antimony contents of primary mantle sulfides, *Can. Mineral.*, *40*(2), 637–650, doi:10.2113/gscanmin.40.2.637.

Hauri, E., J. Wang, J. E. Dixon, P. L. King, C. W. Mandeville, and S. Newman (2002), SIMS analysis of volatiles in silicate glasses 1. Calibration, matrix effects and comparisons with FTIR, *Chem. Geol.*, *183*, 99–114, doi:10.1016/S0009-2541(01)00375-8.

Hergt, J. M., and J. D. Woodhead (2007), A critical evaluation of recent models for Lau–Tonga arc–backarc basin magmatic evolution, *Chem. Geol.*, *245*(1–2), 9–44, doi:10.1016/j.chemgeo.2007.07.022.

Hermann, J., and C. J. Spandler (2008), Sediment melts at subarc depths: An experimental study, *J. Petrol.*, *49*(4), 717–740, doi:10.1093/petrology/egm073.

Hilton, D. R., M. F. Thirlwall, R. N. Taylor, B. J. Murton, and A. Nichols (2000), Controls on magmatic degassing along the Reykjanes Ridge with implications for the helium paradox, *Earth Planet. Sci. Lett.*, *183*(1–2), 43–50, doi:10.1016/S0012-821X(00)00253-3.

Hofmann, A. W. (2003), Sampling mantle heterogeneity through oceanic basalts: Isotopes and trace elements, in *The Mantle and Core*, edited by R. W. Carlson, pp. 61–101, Elsevier-Pergamon, Oxford, U. K.

Jackson, M. G., S. R. Hart, J. G. Konter, A. A. P. Koppers, H. Staudigel, M. D. Kurz, J. Blusztajn, and J. M. Sinton (2010), Samoan hot spot track on a "hot spot highway": Implications for mantle plumes and a deep Samoan mantle source, *Geochem. Geophys. Geosyst.*, *11*, Q12009, doi:10.1029/2010GC003232.

Jenner, F. E., and H. C. O'Neill (2012a), Analysis of 60 elements in 616 ocean floor basaltic glasses, *Geochem. Geophys. Geosyst.*, *13*, Q02005, doi:10.1029/2011GC004009.

Jenner, F. E., and H. C. O'Neill (2012b), Major and trace analysis of basaltic glasses by laser-ablation ICP-MS, *Geochem. Geophys. Geosyst.*, *13*, Q03003, doi:10.1029/2011GC003890.

Jenner, F. E., P. Holden, J. A. Mavrogenes, H. S. C. O'Neill, and C. Allen (2009), Determination of selenium concentrations in NIST SRM 610, 612, 614 and geological glass reference materials using the electron probe, LA-ICP-MS and SHRIMP II, *Geostand. Geoanal. Res.*, *33*(3), 309–317, doi:10.1111/j.1751-908X.2009.00024.x.

Jenner, F. E., H. C. O'Neill, R. J. Arculus, and J. A. Mavrogenes (2010), The magnetite crisis in the evolution of arc-related magmas and the initial concentration of Au, Ag, and Cu, *J. Petrol.*, *51*(12), 2445–2464, doi:10.1093/petrology/egq063.

Jugo, P. J., R. W. Luth, and J. P. Richards (2005), An experimental study of the sulfur content in basaltic melts saturated with immiscible sulfide or sulfate liquids at 1300°C and 1.0 GPa, *J. Petrol.*, *46*, 783–798, doi:10.1093/petrology/egh097.

Kamenetsky, V. S., R. A. Binns, J. B. Gemmell, A. J. Crawford, T. P. Mernagh, R. Maas, and D. Steele (2001), Parental basaltic melts and fluids in eastern Manus backarc Basin: Implications for hydrothermal mineralisation, *Earth Planet. Sci. Lett.*, *184*, 685–702, doi:10.1016/S0012-821X(00)00352-6.

Keller, N., R. J. Arculus, J. Hermann, and S. Richards (2008), Back-arc with arc signatures: Fonualei Rifts, northern Lau Basin, Tonga, *J. Geophys. Res.*, *113*, B08S07, doi:10.1029/2007JB005451.

Klein, E. M. (2003), Geochemistry of the igneous oceanic crust, in *The Crust*, edited by R. L. Rudnick, pp. 433–463, Pergamon, Oxford, U. K.

Klimm, K., J. D. Blundy, and T. H. Green (2008), Trace element partitioning and accessory phase saturation during H_2O-saturated melting of basalt with implications for subduction zone chemical fluxes, *J. Petrol.*, *49*(3), 523–553, doi:10.1093/petrology/egn001.

Koppers, A. A. P., J. A. Russell, J. Roberts, M. G. Jackson, J. G. Konter, D. J. Wright, H. Staudigel, and S. R. Hart (2011), Age systematics of two young en echelon Samoan volcanic trails, *Geochem. Geophys. Geosyst.*, *12*, Q07025, doi:10.1029/2010GC003438.

Kristall, B., D. Nielsen, M. D. Hannington, D. S. Kelley, and J. R. Delaney (2011), Chemical microenvironments within sulfide structures from the Mothra Hydrothermal Field:

Evidence from high-resolution zoning of trace elements, *Chem. Geol.*, *290*(1–2), 12–30, doi:10.1016/j.chemgeo.2011.08.008.

Langmuir, C. H., E. M. Klein, and T. Plank (1992), Petrological systematics of mid-ocean ridge basalts: Constraints on melt generation beneath ocean ridges, in *Mantle Flow and Melt Generation at Mid-Ocean Ridges*, *Geophys. Monogr. Ser.*, vol. 71, edited by J. P. Morgan, D. K. Blackman, and J. M. Sinton, pp. 183–280, AGU, Washington, D. C., doi:10.1029/GM071p0183.

Loock, G., W. F. McDonough, S. L. Goldstein, and A. W. Hofmann (1990), Isotopic compositions of volcanic glasses from the Lau Basin, *Mar. Min.*, *9*, 235–245.

Lupton, J. E., and H. Craig (1975), Excess ^{3}He in oceanic basalts: Evidence for terrestrial primordial helium, *Earth Planet. Sci. Lett.*, *26*(2), 133–139, doi:10.1016/0012-821X(75)90080-1.

Lupton, J. E., R. J. Arculus, R. R. Greene, L. J. Evans, and C. I. Goddard (2009), Helium isotope variations in seafloor basalts from the Northwest Lau Backarc Basin: Mapping the influence of the Samoan hotspot, *Geophys. Res. Lett.*, *36*, L17313, doi:10.1029/2009GL039468.

Lupton, J. E., R. J. Arculus, L. J. Evans, and D. Graham (2012a), Mantle hotspot neon in basalts from the Northwest Lau Back-arc Basin, *Geophys. Res. Lett.*, *39*, L08308, doi:10.1029/2012GL051201.

Lupton, J. E., R. J. Arculus, J. A. Reising, G. J. Massoth, R. R. Greene, L. J. Evans, and N. J. Buck (2012b), Hydrothermal activity in the Northwest Lau Backarc Basin: Evidence from water-column measurements, *Geochem. Geophys. Geosyst.*, *13*, Q0AF04, doi:10.1029/2011GC003891.

Mallmann, G., and H. C. O'Neill (2009), The crystal/melt partitioning of V during mantle melting as a function of oxygen fugacity compared with some other elements (Al, P, Ca, Sc, Ti, Cr, Fe, Ga, Y, Zr and Nb), *J. Petrol.*, *50*(9), 1765–1794, doi:10.1093/petrology/egp053.

Mantovani, E., M. Viti, D. Babbucci, C. Tamburelli, and D. Albarello (2001), Back arc extension: Which driving mechanism?, *J. Virtual Explorer*, *3*, 17–45, doi:10.3809/jvirtex.2001.00025.

Martinez, F., and B. Taylor (2003), Controls on back-arc crustal accretion: Insights from the Lau, Manus and Mariana basins, *Geol. Soc. Spec. Publ.*, *219*(1), 19–54, doi:10.1144/GSL.SP.2003.219.01.02.

Mathez, E. A. (1976), Sulfur solubility and magmatic sulphides in submarine basalt glass, *J. Geophys. Res.*, *81*(23), 4269–4276, doi:10.1029/JB081i023p04269.

Mavrogenes, J. A., and H. C. O'Neill (1999), The relative effects of pressure, temperature and oxygen fugacity on the solubility of sulfide in mafic magmas, *Geochim. Cosmochim. Acta*, *63*(7–8), 1173–1180, doi:10.1016/S0016-7037(98)00289-0.

Morris, J. D., and J. G. Ryan (2003), Subduction zone processes and implications for changing composition of the upper and lower mantle, in *Treatise on Geochemistry*, vol. 2, *The Mantle and Core*, edited by R. W. Carlson, pp. 451–470, Elsevier, Oxford, U. K.

Natland, J. H. (1980), The progression of volcanism in the Samoan linear volcanic chain, *Am. J. Sci.*, *280-A*, 709–735.

Newsom, H. E., W. M. White, K. P. Jochum, and A. W. Hofmann (1986), Siderophile and chalcophile element abundances in oceanic basalts, Pb isotope evolution and growth of the Earth's core, *Earth Planet. Sci. Lett.*, *80*(3–4), 299–313, doi:10.1016/0012-821X(86)90112-3.

Nielsen, S. G., M. Rehkämper, D. A. H. Teagle, D. A. Butterfield, J. C. Alt, and A. N. Halliday (2006), Hydrothermal fluid fluxes calculated from the isotopic mass balance of thallium in the ocean crust, *Earth Planet. Sci. Lett.*, *251*(1–2), 120–133, doi:10.1016/j.epsl.2006.09.002.

Noll, J. P. D., H. E. Newsom, W. P. Leeman, and J. G. Ryan (1996), The role of hydrothermal fluids in the production of subduction zone magmas: Evidence from siderophile and chalcophile trace elements and boron, *Geochim. Cosmochim. Acta*, *60*(4), 587–611, doi:10.1016/0016-7037(95)00405-X.

Norman, M. D., M. O. Garcia, and V. C. Bennett (2004), Rhenium and chalcophile elements in basaltic glasses from Ko'olau and Moloka'i volcanoes: Magmatic outgassing and composition of the Hawaiian plume, *Geochim. Cosmochim. Acta*, *68*(18), 3761–3777, doi:10.1016/j.gca.2004.02.025.

O'Connor, J. M., P. Stoffers, J. R. Wijbrans, and T. J. Worthington (2007), Migration of widespread long-lived volcanism across the Galápagos Volcanic Province: Evidence for a broad hotspot melting anomaly?, *Earth Planet. Sci. Lett.*, *263*(3–4), 339–354, doi:10.1016/j.epsl.2007.09.007.

O'Neill, H. C., and J. A. Mavrogenes (2002), The sulfide capacity and the sulfur content at sulfide saturation of silicate melts at 1400°C and 1 bar, *J. Petrol.*, *43*(6), 1049–1087, doi:10.1093/petrology/43.6.1049.

Pack, A., S. S. Russell, J. M. G. Shelley, and M. van Zuilen (2007), Geo- and cosmochemistry of the twin elements yttrium and holmium, *Geochim. Cosmochim. Acta*, *71*(18), 4592–4608, doi:10.1016/j.gca.2007.07.010.

Palme, H., and H. C. O'Neill (2003), Compositional estimates of mantle composition, in *The Mantle and Core*, edited by R. W. Carlson, pp. 1–38, Elsevier-Pergamon, Oxford, U. K.

Peach, C. L., E. A. Mathez, and R. R. Keays (1990), Sulfide melt-silicate melt distribution coefficients for noble metals and other chalcophile elements as deduced from MORB: Implications for partial melting, *Geochim. Cosmochim. Acta*, *54*(12), 3379–3389, doi:10.1016/0016-7037(90)90292-S.

Pearce, J. A. (2008), Geochemical fingerprinting of oceanic basalts with applications to ophiolite classification and the search for Archean oceanic crust, *Lithos*, *100*, 14–48, doi:10.1016/j.lithos.2007.06.016.

Pearce, J. A., R. C. Stern, S. H. Bloomer, and P. Fryer (2005), Geochemical mapping of the Mariana arc-basin system: Implications for the nature and distribution of subduction components, *Geochem. Geophys. Geosyst.*, *6*, Q07006, doi:10.1029/2004GC000895.

Pearce, J. A., P. D. Kempton, and J. B. Gill (2007), Hf–Nd evidence for the origin and distribution of mantle domains in the SW Pacific, *Earth Planet. Sci. Lett.*, *260*(1–2), 98–114, doi:10.1016/j.epsl.2007.05.023.

Pelletier, B., S. Calmant, and R. Pillet (1998), Current tectonics of the Tonga–New Hebrides region, *Earth Planet. Sci. Lett.*, *164*(1–2), 263–276, doi:10.1016/S0012-821X(98)00212-X.

Pietruszka, A. J., E. H. Hauri, R. W. Carlson, and M. O. Garcia (2006), Remelting of recently depleted mantle within the Hawaiian plume inferred from the ^{226}Ra–^{230}Th–^{238}U disequilibria of Pu'u'Ō'ō eruption lavas, *Earth Planet. Sci. Lett.*, *244*(1–2), 155–169, doi:10.1016/j.epsl.2006.01.039.

Plank, T. (2005), Constraints from thorium/lanthanum on sediment recycling at subduction zones and the evolution of the continents, *J. Petrol.*, *46*(5), 921–944, doi:10.1093/petrology/egi005.

Plank, T., and C. H. Langmuir (1988), An evaluation of the global variations in the major element chemistry of arc basalts, *Earth Planet. Sci. Lett.*, *90*(4), 349–370, doi:10.1016/0012-821X(88)90135-5.

Poreda, R. J. (1985), Helium-3 and deuterium in back-arc basalts: Lau Basin and the Mariana Trough, *Earth Planet. Sci. Lett.*, *73*(2–4), 244–254, doi:10.1016/0012-821X(85)90073-1.

Poreda, R. J., and H. Craig (1992), He and Sr isotopes in the Lau Basin mantle: Depleted and primitive mantle components, *Earth Planet. Sci. Lett.*, *113*(4), 487–493, doi:10.1016/0012-821X(92)90126-G.

Puchtel, I., and M. Humayun (2000), Platinum group elements in Kostomuksha komatiites and basalts: Implications for oceanic crust recycling and core-mantle interaction, *Geochim. Cosmochim. Acta*, *64*(24), 4227–4242, doi:10.1016/S0016-7037(00)00492-0.

Puchtel, I. S., and M. Humayun (2001), Platinum group element fractionation in a komatiitic basalt lava lake, *Geochim. Cosmochim. Acta*, *65*(17), 2979–2993, doi:10.1016/S0016-7037(01)00642-1.

Regelous, M., S. Turner, T. Falloon, P. Taylor, J. Gamble, and T. Green (2008), Mantle dynamics and mantle melting beneath Niuafo'ou Island and the northern Lau back-arc basin, *Contrib. Mineral. Petrol.*, *156*(1), 103–118, doi:10.1007/s00410-007-0276-7.

Richards, S., R. Holm, and G. Barber (2011), When slabs collide: A tectonic assessment of deep earthquakes in the Tonga-Vanuatu region, *Geology*, *39*(8), 787–790, doi:10.1130/G31937.1.

Ripley, E. M., J. G. Brophy, and C. S. Li (2002), Copper solubility in a basaltic melt and sulfide liquid/silicate melt partition coefficients of Cu and Fe, *Geochim. Cosmochim. Acta*, *66*(15), 2791–2800, doi:10.1016/S0016-7037(02)00872-4.

Robinson, J. A. C., and B. J. Wood (1998), The depth of the spinel to garnet transition at the peridotite solidus, *Earth Planet. Sci. Lett.*, *164*(1–2), 277–284, doi:10.1016/S0012-821X(98)00213-1.

Ruscitto, D. M., P. J. Wallace, L. B. Cooper, and T. Plank (2012), Global variations in H_2O/Ce: 2. Relationships to arc magma geochemistry and volatile fluxes, *Geochem. Geophys. Geosyst.*, *13*, Q03025, doi:10.1029/2011GC003887.

Saal, A. E., E. H. Hauri, C. H. Langmuir, and M. R. Perfit (2002), Vapour undersaturation in primitive mid-ocean-ridge basalt and the volatile content of Earth's upper mantle, *Nature*, *419*, 451–455, doi:10.1038/nature01073.

Schellart, W. P. (2004), Kinematics of subduction and subduction-induced flow in the upper mantle, *J. Geophys. Res.*, *109*, B07401, doi:10.1029/2004JB002970.

Schellart, W. P., J. Freeman, D. R. Stegman, L. Moresi, and D. May (2007), Evolution and diversity of subduction zones controlled by slab width, *Nature*, *446*, 308–311, doi:10.1038/nature05615.

Shin, D., H.-I. Park, I. Lee, K.-S. Lee, and J. Hwang (2004), Hydrothermal As–Bi mineralization in the Nakdong deposits, South Korea: Insight from fluid inclusions and stable isotopes, *Can. Mineral.*, *42*(5), 1465–1481, doi:10.2113/gscanmin.42.5.1465.

Sims, K. W. W., H. E. Newsom, and E. S. Gladney (1990), Chemical fractionation during formation of the Earth's core and continental crust: Clues from As, Sb, W and Mo, in *Origin of the Earth*, edited by H. E. Newsom and J. H. Jones, pp. 291–317, Oxford Univ. Press, New York.

Sinton, J. M., L. L. Ford, B. Chappell, and M. T. McCulloch (2003), Magma genesis and mantle heterogeneity in the Manus back-arc basin, Papua New Guinea, *J. Petrol.*, *44*, 159–195, doi:10.1093/petrology/44.1.159.

Skora, S., and J. Blundy (2010), High-pressure hydrous phase relations of radiolarian clay and implications for the involvement of subducted sediment in arc magmatism, *J. Petrol.*, *51*(11), 2211–2243, doi:10.1093/petrology/egq054.

Staudigel, H., K. H. Park, M. Pringle, J. L. Rubenstone, W. H. F. Smith, and A. Zindler (1991), The longevity of the South Pacific isotopic and thermal anomaly, *Earth Planet. Sci. Lett.*, *102*(1), 24–44, doi:10.1016/0012-821X(91)90015-A.

Stegman, D. R., J. Freeman, W. P. Schellart, L. Moresi, and D. May (2006), Influence of trench width on subduction hinge retreat rates in 3-D models of slab rollback, *Geochem. Geophys. Geosyst.*, *7*, Q03012, doi:10.1029/2005GC001056.

Stimac, J., and D. Hickmott (1994), Trace-element partition coefficients for ilmenite, orthopyroxene and pyrrhotite in rhyolite determined by micro-PIXE analysis, *Chem. Geol.*, *117*(1–4), 313–330, doi:10.1016/0009-2541(94)90134-1.

Syracuse, E. M., P. E. van Keken, and G. A. Abers (2010), The global range of subduction zone thermal models, *Phys. Earth Planet. Inter.*, *183*(1–2), 73–90, doi:10.1016/j.pepi.2010.02.004.

Taylor, B., K. Zellmer, F. Martinez, and A. Goodliffe (1996), Sea-floor spreading in the Lau back-arc basin, *Earth Planet. Sci. Lett.*, *144*(1–2), 35–40, doi:10.1016/0012-821X(96)00148-3.

Tian, L., P. R. Castillo, J. W. Hawkins, D. R. Hilton, B. B. Hanan, and A. J. Pietruszka (2008), Major and trace element and Sr–Nd isotope signatures of lavas from the Central Lau Basin: Implications for the nature and influence of subduction components in the back-arc mantle, *J. Volcanol. Geotherm. Res.*, *178*(4), 657–670, doi:10.1016/j.jvolgeores.2008.06.039.

Tian, L., P. R. Castillo, D. R. Hilton, J. W. Hawkins, B. B. Hanan, and A. J. Pietruszka (2011), Major and trace element and Sr-Nd isotope signatures of the northern Lau Basin lavas: Implications for the composition and dynamics of the back-arc basin mantle, *J. Geophys. Res.*, *116*, B11201, doi:10.1029/2011JB008791.

Turner, S., and C. Hawkesworth (1998), Using geochemistry to map mantle flow beneath the Lau Basin, *Geology*, *26*, 1019–1022, doi:10.1130/0091-7613(1998)026<1019:UGTMMF>2.3.CO;2.

Urakawa, S., M. Kato, and M. Kumazawa (1987), Experimental study on the phase relations in the system Fe-Ni-O-S up to 15 GPa, in *High-Pressure Research in Mineral Physics: A Volume in Honor of Syun-iti Akimoto*, *Geophys. Monogr. Ser.*, vol. 39, edited by M. H. Manghnani and Y. Syono, pp. 95–111, AGU, Washington, D. C., doi:10.1029/GM039p0095.

Volpe, A. M., J. D. Macdougall, and J. W. Hawkins (1988), Lau Basin basalts (LBB); trace element and Sr-Nd isotopic evidence for heterogeneity in backarc basin mantle, *Earth Planet. Sci. Lett.*, *90*(2), 174–186, doi:10.1016/0012-821X(88)90099-4.

Weis, D., and F. A. Frey (1996), Role of the Kerguelen Plume in generating the eastern Indian Ocean seafloor, *J. Geophys. Res.*, *101*(B6), 13,831–13,849, doi:10.1029/96JB00410.

Workman, R. K., S. R. Hart, M. Jackson, M. Regelous, K. A. Farley, J. Blusztajn, M. Kurz, and H. Staudigel (2004), Recycled metasomatized lithosphere as the origin of the Enriched Mantle II (EM2) end-member: Evidence from the Samoan Volcanic Chain, *Geochem. Geophys. Geosyst.*, *5*, Q04008, doi:10.1029/2003GC000623.

Workman, R. K., E. Hauri, S. R. Hart, J. Wang, and J. Blusztajn (2006), Volatile and trace elements in basaltic glasses from Samoa: Implications for water distribution in the mantle, *Earth Planet. Sci. Lett.*, *241*(3–4), 932–951, doi:10.1016/j.epsl.2005.10.028.

Wykes, J. L., H. C. O'Neill, and J. A. Mavrogenes (2011), XANES investigation of selenium speciation in silicate glasses, paper presented at Annual V.M. Goldschmidt Conference, Mineral. Mag., Prague.

Yi, W., A. N. Halliday, J. C. Alt, D.-C. Lee, M. Rehkämper, M. O. Garcia, C. H. Langmuir, and Y. Su (2000), Cadmium, indium, tin, tellurium, and sulfur in oceanic basalts: Implications for chalcophile element fractionation in the Earth,

J. Geophys. Res., *105*(B8), 18,927–18,948, doi:10.1029/2000JB900152.

Zellmer, K. E., and B. Taylor (2001), A three-plate kinematic model for Lau Basin opening, *Geochem. Geophys. Geosyst.*, *2*(5), 1020, doi:10.1029/2000GC000106.

Zhang, N., and R. N. Pysklywec (2006), Role of mantle flow at the North Fiji Basin: Insights from anomalous topography, *Geochem. Geophys. Geosyst.*, *7*, Q12002, doi:10.1029/2006GC001376.